

Circum-Antarctic Glacially Induced Fault Reactivation Since the Last Glacial Maximum



Key Points:

- We investigate stress-model combinations indicating fault reactivation in the Antarctic plate triggered by glacially induced stress changes
- Glacially triggered faulting may have occurred since the Last Glacial Maximum in many inherited Antarctic rift systems
- Fault instability is higher for a strike-slip faulting stress regime than for a thrust faulting stress regime in Antarctica

Supporting Information:

Supporting Information may be found in the online version of this article.

Correspondence to:

C. Hübscher,
christian.huebscher@uni-hamburg.de

Citation:

Barbosa, I., Steffen, R., Steffen, H., Seidel, E., Gohl, K., & Hübscher, C. (2025). Circum-Antarctic glacially induced fault reactivation since the Last Glacial Maximum. *Tectonics*, *44*, e2024TC008464. <https://doi.org/10.1029/2024TC008464>

Received 12 JUN 2024
Accepted 13 MAR 2025

Ingra Barbosa¹ , Rebekka Steffen^{2,3} , Holger Steffen² , Elisabeth Seidel¹, Karsten Gohl⁴ , and Christian Hübscher¹ 

¹Institute of Geophysics, University of Hamburg, Hamburg, Germany, ²Geodetic Infrastructure, Lantmäteriet, Gävle, Sweden, ³Department of Earth and Environmental Sciences, Dalhousie University, Halifax, NS, Canada, ⁴Alfred Wegener Institute Helmholtz-Centre for Polar and Marine Research, Bremerhaven, Germany

Abstract Glacial isostatic adjustment (GIA) has the potential to reactivate faults in the crust due to the generation of stresses caused by changes in the ice load. Research on the release of stress along pre-existing faults, known as glacially induced faults, in Antarctica is limited due to the lack of detailed information about the region's ice sheet history, Earth's rheology, and fault parameters. Here, we analyse the reactivation potential of 62 faults since the Last Glacial Maximum (LGM) by calculating Coulomb failure stress changes (Δ CFS) for a thrust faulting and a strike-slip faulting stress regime in combination with various GIA models and stress parameters. In general, a higher fault instability was observed in a strike-slip faulting stress regime compared to a thrust faulting stress regime. Furthermore, the ice sheet history models had a higher effect on fault instability than the Earth models. Faults located in the Ross Sea area show the highest potential of fault reactivation, while those in the Antarctic Peninsula show the lowest. Our results suggest that the potential for glacially triggered faulting has increased since the LGM in many inherited rift systems, and some faults remain unstable until today.

1. Introduction

Glacial isostatic adjustment (GIA) is the response of the Earth to the redistribution of masses following the advance or retreat of glaciers and ice sheets (Wu & Peltier, 1982). Although this process affects the entire globe, it has a prominent effect in North America, northern Europe and in the still glaciated regions of Greenland and Antarctica. Changes in the redistribution of masses on the Earth's surface affect the gravitational potential, displacement field and rotational state of the Earth (Milne et al., 1998; Peltier, 1974; Whitehouse et al., 2019). In addition, ice load variations also cause stress changes due to the vertical load itself and flexural stresses due to the bending of the lithosphere (R. Steffen, Wu, & Lund, 2021). Following commonly used GIA terminology, the lithosphere comprises the crust and upper solid mantle, while the mantle encompasses the asthenosphere down to the lower mantle. The lithosphere in GIA is defined to react elastically on time scales of a few 100,000 years, while the mantle behaves viscoelastically. This rheological behavior leads to a third stress component, which comes from the migration of stresses from the mantle to the lithosphere. These stresses were generated in the mantle during the early phases of glacial loading when the mantle reacted elastically (R. Steffen, Wu, & Lund, 2021). The sum of these glacially induced stress changes might cause previously existing faults to become unstable and be reactivated. This process, called glacially triggered faulting, can happen thousands of years after a deglaciation period (Brandes et al., 2015; R. Steffen, Wu, & Lund, 2021) and may occur up to a few hundred kilometers away from glaciated areas (Wu et al., 2021).

Glacially triggered faulting is well recorded in northern Europe and concerns an area larger than the previously glaciated region, for example, also the surrounding area of the Fennoscandian Ice Sheet in Germany, Poland and the Czech Republic (Brandes et al., 2018; Lagerbäck & Sundh, 2008; Müller et al., 2021; Pisarska-Jamroży et al., 2022; Štěpančíková et al., 2022). There are dozens of so-called glacially induced faults (GIFs) that were reactivated mainly at the end or soon after the deglaciation (H. Steffen, Olesen, & Sutinen, 2021). Outside of Europe the record of GIFs is sparse (Munier et al., 2020; R. Steffen et al., 2020). In Antarctica, there are a few suggestions of GIFs that were never fully investigated (H. Steffen & Steffen, 2021a).

In general, the lack of consistent long-term observation in Antarctica presents difficulties in the analysis of its glacial history and in the prediction of how the current world climate trends might affect the continent (Casado et al., 2023; Nicolas & Bromwich, 2014; Schroeder et al., 2019). Although research about GIA in Antarctica can

© 2025. The Author(s).

This is an open access article under the terms of the [Creative Commons Attribution License](https://creativecommons.org/licenses/by/4.0/), which permits use, distribution and reproduction in any medium, provided the original work is properly cited.

still be considered scarce, there is a rising number of recent studies aimed at improving model quality (e.g., Bagge et al., 2021; Li et al., 2020; Nield et al., 2018; Powell et al., 2022; van der Wal et al., 2023). Such advanced GIA models include sophisticated ice sheet history models and a 3D subsurface structure that can help understand the glacial influence on the regional stress field and thus potential fault reactivation in the past.

Antarctica has a long faulting history as it suffered multiple rifting episodes since its generation in the aftermath of the Gondwana break-up (Jordan et al., 2020; Storey & Granot, 2021). Faulting is reported both onshore and offshore (Carson, 2012; Sauli et al., 2021); the later mainly by the interpretation of marine seismic profiles. Most of the continent is covered by the Antarctic Ice Sheet (AIS), which reached its Last Glacial Maximum (LGM) between 26.0 and 18.0 ka before present (BP) (Golledge et al., 2012; Larter et al., 2014; Rhee et al., 2022). The weight of the ice alters the pre-existing stress fields, favoring a suppression of seismicity (Johnston, 1987). Changes in the ice sheet affect the stress conditions, which might lead to an increase in seismic activity.

Identifying potential sources of tectonic changes resulting from GIA could aid in a deeper understanding of how past glacial events have impacted seismotectonics in Antarctica and how current climatic trends may further influence it. We evaluate the potential for glacially triggered faulting in Antarctica by analysing glacially induced stresses at faults identified in marine seismic profiles and in the literature. The glacially induced stresses are obtained using different GIA models and various potential stress field settings to determine the impact of GIA on each identified fault in terms of stress changes for the last 21,000 years. In the following, we first illuminate the geological and glacial history of Antarctica. Then we introduce our GIA modeling and stress analysis. In Section 4, we present the potential for glacially induced reactivation of the identified faults. We discuss our results in Section 5 and conclude in Section 6.

2. Geological and Glacial History

The Antarctic continent is located centrally in the Antarctic tectonic plate, which is surrounded mostly by spreading ridges and passive margins. The continent is commonly subdivided into two regions (Figure 1): the older and mostly cratonic East Antarctica (Harley et al., 2013), and the younger and more tectonically active West Antarctica (Jordan et al., 2020). The few focal mechanism available seem to indicate an intraplate predominance of normal faulting events in continental East Antarctica (Lough et al., 2018), but thrust (Ekström et al., 2012) and strike-slip faulting (Reading, 2007) in coastal and marine Antarctica. Since the LGM, ice sheet retreat has occurred discontinuously episodically across Antarctica (Bentley et al., 2014; R. S. Jones et al., 2022; Tigchelaar et al., 2019). In the following subsections we will discuss five regions of Antarctica, separated due to their distinct geological and glacial history. Supporting Information S1 includes detailed maps of each research area and references related to the tectonic background reported in Figure 1.

2.1. Antarctic Peninsula

The Antarctic Peninsula is the most tectonically active region of Antarctica. Its northern part is located in a tectonic margin that underwent episodes of magmatism from early Ordovician until the Neogene (Burton-Johnson & Riley, 2015; Jordan et al., 2020). In the southwest, a predominance of a strike-slip faulting stress regime was suggested by Maestro and López-Martínez (2011).

The ice sheet extended to the continental shelf-edge during the LGM and started retreating at c. 20.0 ka BP (Glasser et al., 2014). Radiocarbon data support that in the South Shetland Islands, north of the Antarctic Peninsula, deglaciation started at 11.0 ka BP and continued until 4.7 ka BP (Watcham et al., 2011). In the southwest, thinning of the ice coverage lasted from 22.0 ka BP until at least 7.4 ka BP in the surrounding areas of George VI Sound (Bentley et al., 2006).

2.2. Amundsen and Bellingshausen Seas

Recurring Cenozoic rifting within the West Antarctic Rift System has led to branches in parts of the Amundsen Sea and Bellingshausen Sea sectors. This activity, as derived from geophysical data and inferred faulting, resulted in a regionally thinned crust accompanied by magnetic anomalies (Dziadek et al., 2021; Gohl et al., 2013).

During the LGM the grounded ice reached or approximated the continental shelf edge of the Amundsen and Bellingshausen seas (Larter et al., 2014). Carbon dating indicates that deglaciation of the ice shelf started before 22.3 ka BP and reached the Amundsen Sea mid-shelf by c. 13.8 ka BP (Smith et al., 2011). Deglaciation of the

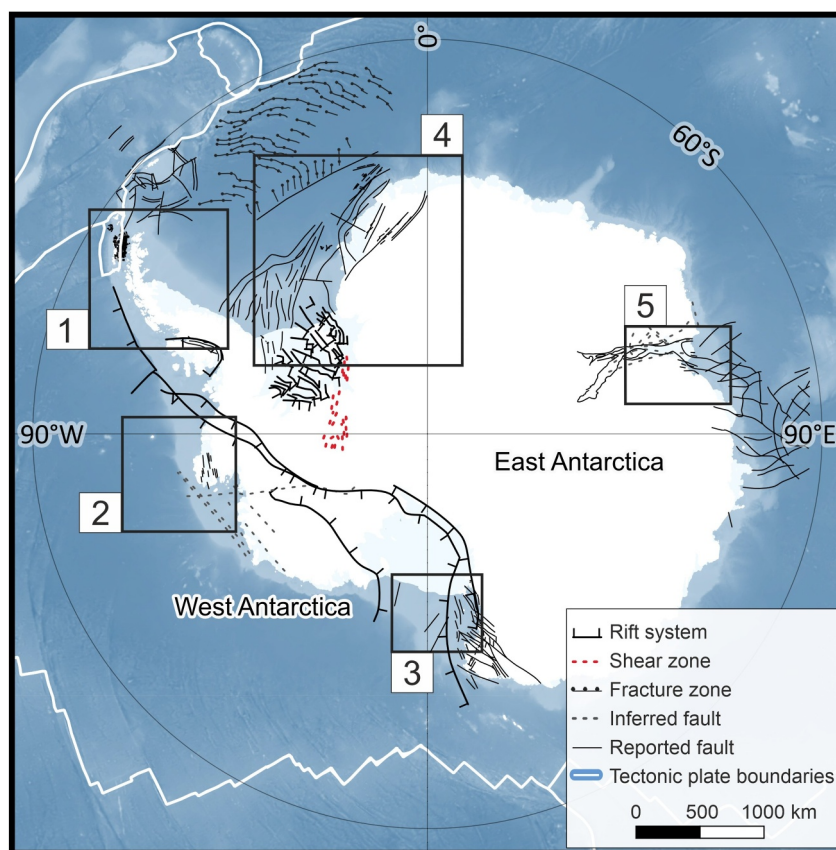


Figure 1. Tectonic overview of Antarctica and the research areas of this study. (1) Antarctic Peninsula; (2) Amundsen and Bellingshausen seas; (3) Ross Sea; (4) Lazarev and Weddell seas; (5) Prydz Bay.

inner continental shelf started before 13.0 ka BP (Klages et al., 2014; Lamping et al., 2020) and lasted until c. 6.3 ka BP (Hillenbrand et al., 2010).

2.3. Ross Sea

The Ross Sea is dominated by the West Antarctic Rift System with extended and thinned continental crust that underwent multiple rifting events since the Gondwana breakup (Divenere et al., 1996; Storey et al., 1999). This resulted in complex internal crustal structures with numerous normal and strike-slip faulting in the region (Rocchi et al., 2003; Salvini et al., 1997; Wilson & Paulsen, 2001). In the southwestern Ross Sea, the Terror Rift is dominated by normal faults (Blocher, 2017; Sauli et al., 2021).

At the LGM the grounded ice shelf reached the outer shelf and most of the deglaciation occurred after 13.0 ka BP (Anderson et al., 2014; Heath et al., 2022). There was a slow retreat of the ice to the center-west Ross Sea by c. 11.0 ka BP and a fast one to the south between 11.0 and 10.0 ka BP. The grounded ice continued retreating in the south until c. 3.0–2.0 ka BP. In the north, the ice reached the vicinity of its present extent c. 7.5 ka BP.

2.4. Lazarev and Weddell Seas

The Gondwana break-up in the Early Jurassic most likely caused the extension that generated the Weddell Sea Rift System (Dalziel et al., 2000; Elliot et al., 1999). Using paleo-magnetic data and tectonic reconstructions, Jordan et al. (2013) theorized there is a predominance of a strike-slip faulting stress regime in the area. The Lazarev Sea to the east of the Weddell Sea has been associated with intense phases of volcanism and multiple rifting episodes (Hinz et al., 2004).

The behavior of the ice sheets in the Weddell Sea is not well constrained for the Late Quaternary (Arndt et al., 2020; Nichols et al., 2019). It has been suggested that the grounding line might have fluctuated after the

LGM (Hillenbrand et al., 2014; Larter et al., 2012) due to GIA and ice shelf re-settling (Hodgson et al., 2019; Siegert et al., 2019).

In the Lazarev Sea, it is assumed that the ice had its largest extent between 30.0 and 25.0 ka BP (Anderson et al., 2002; Ingólfsson, 2004). Deglaciation from the continental shelf started between 11.9 and 10.8 ka BP (Gingele et al., 1997) and continued until it reached onshore regions c. 3.0 ka BP (Phartiyal et al., 2011).

2.5. Prydz Bay

Prydz Bay is located offshore of the large Lambert Graben in East Antarctica. The area has undergone rifting as part of the East Antarctic Rift System (Lisker et al., 2003; Tochilin et al., 2012) and despite no information on its current stress regime, it is reported to have mostly normal faults (Stagg, 1985).

Geological records from Prydz Bay suggest a maximum extent of grounded ice toward the shelf edge during the LGM (Domack et al., 1998; O'Brien et al., 1999). White et al. (2022) stated that the eastern Prydz Bay was free of grounded ice by c. 14.0 ka BP. Deglaciation at central Prydz Bay started at c. 13.0 ka BP and in Prydz Channel between 18.0 and 12.0 ka BP (Mackintosh et al., 2014).

3. Methods

3.1. Fault Identification

The analysis of the potential fault reactivation requires knowledge about the location (geographical coordinates), as well as strike (φ) and dip (δ) angles of a fault. For our analysis, we focused on identifying faults in offshore regions, where seismic profiles provided more accurate data for evaluating the necessary parameters. Faults were selected based on a literature review of interpreted faults from seismic profile analyses. The seismic profiles used are available through the Antarctic Seismic Data Library System (2024) and fault interpretation was carried out in the Software Kingdom (S&P Global, 2024). Seismic profiles with the identified fault are called profile 1, and supporting profiles parallel or adjacent to profile 1 are called profile 2 (Figure 2). The latter were used to identify the strike of the fault.

Faults in profile 1 were picked manually following the identification in the original literature (Figure 2a). If the same fault was identified in profile 2, a fault map with a grid of locations corresponding to longitude, latitude and depth in two-way-travel-time of the fault plane was produced (Figure 2b). This information was used to obtain fault strike and dip angles. Each fault was given a fault identification number (FID).

The dip was estimated by the angle of the fault in the seismic section (α) of profile 1 (Equation 1) and its relationship to the angle between the seismic section and the fault plane (γ , Equation 2):

$$\alpha = \arctan\left(\frac{y_1 - y_0}{2} \cdot v_{mean} \cdot \sqrt{(x_1 - x_0)^2 + (y_1 - y_0)^2}\right), \quad (1)$$

$$dip = \arctan\left(\frac{\tan(\alpha)}{\tan(\gamma)}\right). \quad (2)$$

x_1 and y_1 correspond to the location of the fault at the deepest point and x_0 and y_0 to the location at the shallowest point. A mean seismic wave velocity v_{mean} of 2,000 m/s is assumed, which is reasonable for our study area (An et al., 2015a, 2015b; Geletti & Busetti, 2011; Mooney et al., 2002; Wonik et al., 2008). For seismic profiles with no supporting profiles, the strike angle was obtained through the direction given in the literature and the dip angle from profile 1. For well recorded faults with no seismic profiles available, the strike angle was obtained from the trend of the fault trace from published maps (Table S2) and dip angles of 45°, 60°, and 75° were used in the calculations. Strike and dip angles were grouped in intervals of 15° between 0–180° (strike) and 0–90° (dip), with a fault geometry characterized by its strike/dip. Faults in the seismic profile were located between 0 and 5 km depth.

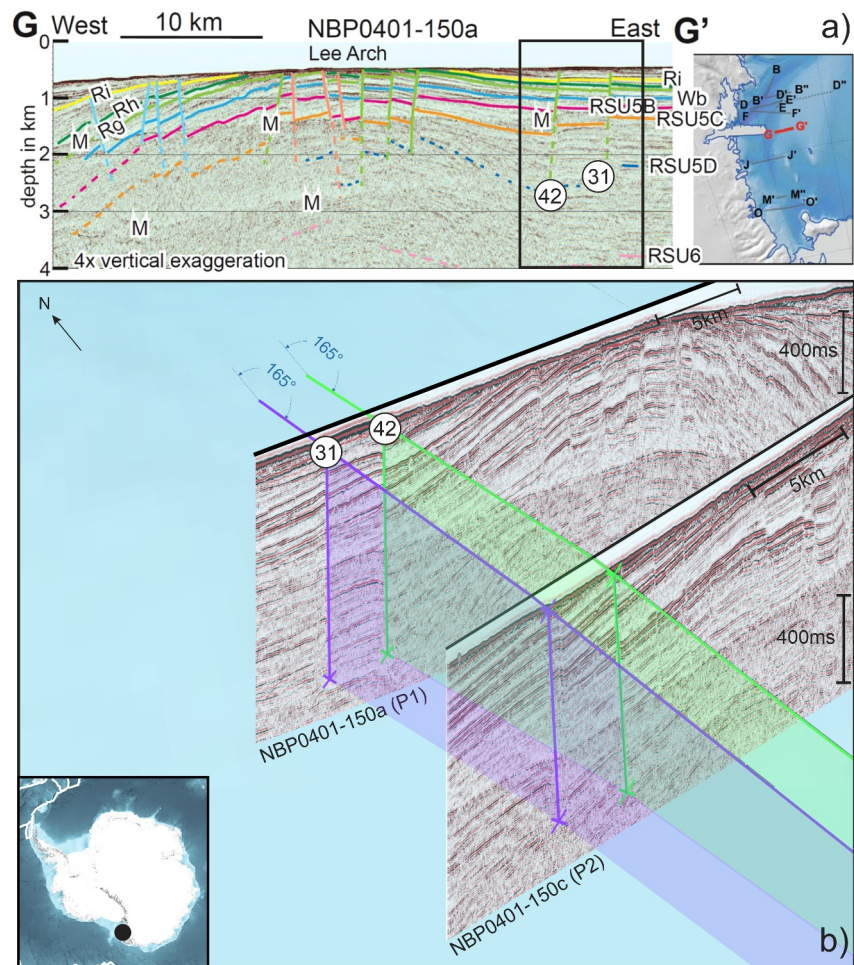


Figure 2. Example of fault identification. (a) Original seismic profile (profile 1) and faults identified by Sauli et al. (2021). Identified faults are marked with a black box and fault identification number (FID). (b) Location of faults indicated by a black dot on the map. Strike angle indicated in the map. Fault map produced by the identification of the faults in profile 1 (P1) and profile 2 (P2) based on Sauli et al. (2021). In purple: FID 31; in green: FID 42. Proportions exaggerated for clarity.

3.2. Modeling of Glacially Induced Stresses

Calculation of glacially induced stresses requires a 3D GIA model that consists of a subsurface structure (Earth model) loaded by an ice sheet history model (ice model). This study employs 21 GIA models to evaluate the potential for glacially triggered faulting in Antarctica. It does not aim to provide a best-fitting GIA model of Antarctica, and therefore Earth and ice models will be discussed rather generally only. An overview of the major differences and example figures for the ice and Earth models are included in Supporting Information S1.

The GIA modeling is based on a non-self-gravitating, Cartesian type Earth model using the commercial finite element (FE) Software Abaqus (Dassault Systemes, 2024). The model space under investigation is limited to a diameter of 6,000 km, but the FE analysis is extended to 56,000 km laterally to avoid boundary effects. The elements have a horizontal dimension of 50 km or 75 km (depending on the applied ice model) in the upper 420 km and a side length of 150 km at larger depths. The Earth models extend from the Earth's surface to the core-mantle boundary to account for stress migration and viscoelastic movement of the mantle. The models consist of 20 depth layers whose vertical side lengths range between 5 km in the upper crust and about 40 km in the lower mantle. This modeling approach has been used in several GIA stress studies (Brandes et al., 2012, 2018; Lund et al., 2009; Pisarska-Jamroży et al., 2019). For more details about the FE modeling the reader is referred to H. Steffen et al. (2019), R. Steffen and Steffen (2021b), and Wu et al. (2021).

The set of Earth models consists of one 1D model (lithosphere and mantle vary vertically) and 10 3D-3D models (lithosphere and mantle vary vertically and horizontally). The 1D model consists of a 120 km thick elastic lithosphere, no asthenosphere, a viscosity of 6×10^{19} Pa s in the upper mantle and 3×10^{21} Pa s in the lower mantle. The 3D mantle structure was constructed using the global seismic tomography model SMEAN2 (Becker & Boschi, 2002; Jackson et al., 2017; Ritsema et al., 2011; Simmons et al., 2010) and five different 1D background viscosity structures: K05 (Kaufmann et al., 2005), OM13 (Okuno & Miura, 2013), VM2 (Peltier, 2004), VM5a (Argus et al., 2014) and W12back (Whitehouse et al., 2012). The 3D seismic structure is converted to viscosity following Wu et al. (2013) using the 1D background viscosity structure and other parameters that vary with depth (activation energy, activation volume, pressure, background temperature profile and relation of the fractional perturbation of shear waves to temperature including effects of both anharmonicity and anelasticity). All models are further multiplied with two different β factor profiles which represents scaling factors regarding the contribution of thermal effects on seismic shear velocities in the mantle and lithosphere (Li et al., 2018). The full 3D viscosity models and more information regarding their generation can be found in R. Steffen and Steffen (2024). 3D mantle models were combined with the 3D lithosphere of model ANT-20 from Lloyd et al. (2020). The elastic parameters Young's modulus, Poisson ratio and density are taken from the Preliminary Reference Earth Model (PREM, Dziewoński & Anderson, 1981).

The two ice models used for the modeling of the AIS history were W12 from Whitehouse et al. (2012) and IJ05_R2 from Ivins et al. (2013). Both models use nearly the same data as input; however, the way they approach the data and construct the model impacts the ice sheet thickness. In order to properly define the time-dependent GIA response, both ice models assume that the loading phase of the Antarctica ice sheet occurred for a period of 100,000 years. Ice model IJ05_R2 has a higher upper bounding limit to the ice volume than W12, and a larger ice extent at the LGM. The stress analysis was done for the time span from 21 ka BP until present (1950) with intervals of 1 ka. This is because both models are, due to the lack of constraining data, very uncertain before that time and contain only a few time steps. The horizontal resolution of the ice model controlled the horizontal resolution of the finite elements in the Earth models with 50 km for IJ05_R2 and 75 km for W12.

Since most identified faults are offshore, changes in the ocean load (due to mass exchange and gravitational effects) must also be considered when analysing glacially induced stresses. Ocean load changes were computed externally using a so-called 1D spherical, compressible GIA model that solves the sea-level equation (Kaufmann, 2004) with a horizontal resolution of approximately 100 km, accounting for ocean changes due to the waxing and waning of ice sheets. The ocean load is calculated for each corresponding time step of the ice load, rescaled to the high resolution grid of the 3D FE model and implemented as load together with the ice model.

3.3. Stress and Coulomb Failure Stress Changes

Stress in the crust can be described by three principal stresses: minimum (S_3), intermediate (S_2), and maximum (S_1) stresses. At the Earth's surface, the principal stresses can be aligned with the vertical and horizontal directions due to the requirement that there are no shear stresses at the free surface. This results in one of the principal stresses being the vertical stress (S_V), and the other two being the maximum horizontal (S_{Hmax}) and minimum horizontal stress (S_h). The anisotropy between these establishes three stress regimes: normal faulting ($S_V > S_{Hmax} > S_h$), strike-slip faulting ($S_{Hmax} > S_V > S_h$) and thrust faulting ($S_{Hmax} > S_h > S_V$) stress regime.

Considering a critically stressed crust, the three principal stresses are related via S_1 , S_2 , and S_3 in Supporting Information S1 and the stress ratio R (Etchecopar et al., 1981):

$$R = \frac{S_1 - S_2}{S_1 - S_3}. \quad (3)$$

Using the stress ratio R , determining the overburden pressure, the gravity, and the depth at a point, the magnitudes of the three principal stresses can be estimated for each stress regime, assuming the principal stresses align with the x-, y-, and z-direction.

Fault reactivation is dependent on the stress accumulation, fault orientation, background stress regime, and friction. A force acting on the area of a fault generates both shear (τ) and normal stress (σ), which are dependent on n , a normal vector to the fault plane. If the shear stress reaches the minimum value required to induce fault slip (known as the Critical Resolved Shear Stress) the fault may be reactivated. With regard to reactivation, a fault can

be optimally oriented, meaning its geometry is closer to failure than any other one for that particular stress regime, or non-optimally oriented, which comprises all other orientations (Sibson, 1985). In an intraplate setting, the crust is often considered to be in a state of frictional faulting equilibrium, making it reasonable to assume that it is critically stressed and thus close to a state of failure (G. C. P. King et al., 1994; R. Steffen et al., 2014; M. D. Zoback & Townend, 2001; M. L. Zoback & Zoback, 2007). The assumption of a critically stressed crust is valid for optimally oriented faults. Thus, faults with orientations that deviate from optimal are not critically stressed. We consider this as a valid assumption, even for Antarctica, as otherwise earthquakes are in general not likely. We assume a critically stressed crust before the onset of glaciation in our modeling.

Changes in the stress field can be correlated to the glacial history through changes in the Coulomb failure stresses (CFS, R. Steffen & Steffen, 2021b). The CFS can be used to evaluate the potential of a reactivation of a fault and is estimated by (Harris, 1998; Reches, 1987):

$$CFS = \tau - \mu \cdot \sigma_n, \quad (4)$$

in which μ is the coefficient of friction.

Decomposing fault strike and dip angles in x-, y- and z-directions of an orthogonal projection, we can estimate the normal vector n of the specific fault (Fossen, 2016; Twiss & Moores, 2007):

$$\begin{aligned} n_x &= \cos \varphi \cdot \sin \delta, \\ n_y &= -\sin \varphi \cdot \sin \delta, \\ n_z &= \cos \delta. \end{aligned} \quad (5)$$

With this, the CFS can be defined as a function of dip and strike of the fault, the stress ratio and the stress regime. Here we use ΔCFS to describe changes in the stress of a fault in different time periods. Positive ΔCFS are associated with a decrease in the stability of the fault and therefore a higher likelihood of fault reactivation. Negative ΔCFS are associated with an increase of stability and a lower chance of fault reactivation (Hettema, 2020; Qin et al., 2018; Stein, 1999). Fault-geometry-depending changes in normal and shear stress can be estimated allowing the possibility to analyse ΔCFS for both optimally and non-optimally oriented faults (R. Steffen & Steffen, 2021b). However, only optimally oriented faults are considered to be critically stressed and all other faults are stable with a ΔCFS below 0 MPa before the onset of glaciation. Hence, larger glacially induced stresses would be needed to reactivate non-optimally oriented faults than for the reactivation of critically stressed optimally oriented faults.

Strike-slip and thrust faulting stress regimes were applied as background stress regimes when calculating ΔCFS . A normal faulting stress regime was not investigated, as it is typically associated with promoting stability in regions beneath current or former ice sheets (R. Steffen, Wu, & Lund, 2021). Direct observations of background stress information are, strictly speaking, non-existent for Antarctica (Heidbach et al., 2018; Kaufmann et al., 2005; Maestro et al., 2008). The few focal mechanisms available for offshore Antarctica indicate a prevailing thrust or strike-slip stress regime in our research areas (see Section 2). To represent possible background stress realities in the model, each fault was modeled for four maximum horizontal stress (S_{Hmax}) directions of 0° , 45° , 90° , and 135° and stress ratios (R) of 0.05, 0.5, and 0.95 (R. Steffen & Steffen, 2021b). Stresses were calculated at a depth of 2.5 km. Glacially induced stresses reach their maximum at the Earth's surface, and decrease with depth up to a neutral plane where stress directions are inverted and increase again toward the lithosphere-mantle boundary. The existence of surface rupturing in Fennoscandia (Ahmadi et al., 2015; Olesen et al., 1992) and the occurrence of the Ungava earthquake (Canada) at a maximum depth of 3 km (Bent, 1994) support the choice of using 2.5 km to evaluate the glacially induced stress changes. The ΔCFS behavior is similar at larger depths (e.g., 7.5 or 12.5 km) but ΔCFS values are a bit smaller (Pisarska-Jamrozý et al., 2022). For consistency, we use a depth of 2.5 km. The coefficient of friction is set to $\mu = 0.6$, which is a reasonable value for most rock types (Scholz, 2019; Sibson, 1990).

All in all, the modeling consists of several steps. After calculating the GIA response for each GIA model, glacially induced stress changes are computed at each time step. Then, background stresses are generated for each GIA

model by combining various S_{Hmax} directions, stress ratios, and stress regimes. Lastly, the strike and dip angles of each fault, along with the stress field, are used to calculate the ΔCFS .

In total, 504 different stress-model combinations are used (252 each for the strike-slip and thrust faulting stress regimes). Together with the range of strike and dip values, a total of 30,240 combinations is used to analyse the potential of a reactivation at each time step. For each fault identification number (FID), the number of combinations indicating fault reactivation (NCFR) were obtained by the estimation of the ΔCFS assuming an initially critically stressed crust ($CFS_{before\ glaciation} = 0$). At every time step, the ΔCFS of each FID was calculated for all 504 stress-model combinations. If a fault was found to have a positive ΔCFS at least once during the last 21,000 years, the NCFR was increased by one. If ΔCFS was positive several times for one stress-model combination, this combination was only accounted for once in the total NCFR. This means a fault with a potential of reactivation has a minimum NCFR of one, and a maximum of 252 for each stress regime.

4. Results

A total of 38 faults were identified in seismic profiles. Additional nine faults were identified in the literature with no available seismic sections and therefore tested for different dip ranges. Table 1 describes the faults tested in the model and the NCFR of each fault for each stress regime in the last 21,000 years. For more details about the faults, consult Supporting Information S1.

In both ice models the total NCFR is similar for most FIDs, however, the results vary by time step (Figure 3). The 1D Earth model presents lower NCFR than the 3D cases. The β factor does not alter the results in a discernible way, with 99% of the results presenting the same NCFR. The ice models have a larger impact on the potential of fault reactivation than the Earth models. The steepest increase in ΔCFS values was observed when there was a quick decrease in the ice load above the faults, or in the close vicinities to it.

Forty eight out of 62 FIDs present a higher potential of reactivation within a strike-slip faulting stress regime (Figure 3, top). In such a stress regime 54% of the NCFR is for a stress ratio of $R = 0.05$, 28% for $R = 0.5$ and 18% for $R = 0.95$. The Antarctic Peninsula has the lowest NCFR from the investigated research areas.

In a thrust faulting stress regime, 57% of the NCFR is for a stress ratio of $R = 0.95$, 16% for $R = 0.5$ and 27% for $R = 0.05$. Most of the tendency for glacially triggered faulting for this stress regime is in the Amundsen and Bellingshausen seas region, whilst the Antarctic Peninsula, Lazarev Sea and the Weddell Sea regions have zero NCFR for the parameters given (Figure 3, bottom). We present the results of the different areas in more detail next.

4.1. Antarctic Peninsula

The Antarctic Peninsula region has nine identified faults (Figure 4; FIDs 12–20). Of these, FIDs 12–16, north of the Antarctic Peninsula, were initially covered by c. 400 m of ice in the W12 model, which rapidly retreated entirely between 20 and 19 ka BP. According to IJ05_R2, the area was covered by a few meters of ice until 10 ka BP, followed by a complete retreat until present. In a thrust faulting stress regime none of these faults had a potential of reactivation, whilst in a strike-slip faulting regime all of them but for FID 14 presented low positive ΔCFS values for at least 1 time step. In a strike-slip faulting stress regime FIDs 12 (NCFR = 10) and 13 (NCFR = 16) showed the steepest increase in ΔCFS with the decrease of ice (c. 20–18 ka BP) for model W12, but with no potential of reactivation in the present time. Using ice model IJ05_R2, the ΔCFS increased slightly for FIDs 12, 13, 15 (NCFR = 5) and 16 (NCFR = 2) during deglaciation in the surrounding areas until instability was reached for all faults at c. 5 ka BP and continued until present.

4.2. Amundsen and Bellingshausen Seas

In the Amundsen and Bellingshausen seas 11 faults were identified (Figure 5; FIDs 1–11). FIDs 1, 4, 5, 6, 7, and 8 are located outside of the continental shelf and have no grounded ice at any point in time according to both ice models. FID 1 (NCFR = 71) and 4 (NCFR = 72) have a geometry which is optimally oriented for $S_{Hmax} = 90^\circ$ in a thrust faulting stress regime. For a stress ratio of $R = 0.05$, both also had a potential of reactivation for a $S_{Hmax} = 135^\circ$ and $S_{Hmax} = 45^\circ$ from 21 to 18 ka BP, which was a period of intensified deglaciation in the area.

Table 1
Identified Faults, Along With Their Strike and Dip Angles and Potential for Reactivation

FID	Region	Longitude	Latitude	Strike	Dip	TF	SSF
1	Amundsen Sea	-104.621	-68.728	91	25	71	0
2	Amundsen Sea	-112.061	-72.975	145	35	0	0
3	Amundsen Sea	-111.617	-73.311	155	61	10	105
4	Amundsen Sea	-104.480	-68.724	89	30	72	0
5	Bellingshausen Sea	-91.641	-66.852	74	23	92	0
6	Bellingshausen Sea	-91.588	-66.860	74	63	0	24
7	Bellingshausen Sea	-90.814	-66.987	77	38	0	0
8	Bellingshausen Sea	-90.685	-67.007	77	13	0	0
9 ^a	Amundsen Sea	-103.289	-72.606	166	80	11	85
10 ^a	Amundsen Sea	-103.289	-72.606	166	65	8	75
11 ^a	Amundsen Sea	-103.289	-72.606	166	50	0	12
12	Antarctic Peninsula	-57.329	-61.406	22	67	0	10
13	Antarctic Peninsula	-57.451	-61.215	44	61	0	16
14	Antarctic Peninsula	-57.267	-61.203	113	59	0	0
15	Antarctic Peninsula	-57.247	-61.201	97	60	0	5
16	Antarctic Peninsula	-57.222	-61.198	98	66	0	2
17 ^a	Antarctic Peninsula	-69.300	-70.042	115	55	0	0
18 ^b	Antarctic Peninsula	-69.300	-70.042	115	40	0	0
19 ^a	Antarctic Peninsula	-67.502	-71.158	114	55	0	0
20 ^b	Antarctic Peninsula	-67.502	-71.158	114	40	0	0
21	Prydz Bay	75.031	-68.995	130	72	0	71
22	Prydz Bay	75.447	-66.417	134	72	0	68
23	Prydz Bay	74.956	-68.929	109	79	13	105
24	Prydz Bay	75.424	-66.401	137	20	0	0
25 ^a	Prydz Bay	68.599	-71.323	158	80	0	39
26 ^a	Prydz Bay	68.599	-71.323	158	65	0	26
27 ^a	Prydz Bay	68.599	-71.323	158	50	0	0
28 ^a	Prydz Bay	67.977	-73.102	157	80	0	39
29 ^a	Prydz Bay	67.977	-73.102	157	65	0	41
30 ^a	Prydz Bay	67.977	-73.102	157	50	0	12
31	Ross Sea	167.337	-75.720	158	53	3	105
32	Ross Sea	166.748	-75.241	169	68	11	112
33	Ross Sea	166.503	-75.228	144	79	21	95
34	Ross Sea	165.513	-75.149	167	64	0	101
35	Ross Sea	165.268	-76.055	167	70	1	105
36	Ross Sea	165.353	-76.056	179	51	0	21
37	Ross Sea	164.252	-76.040	166	53	0	65
38	Ross Sea	165.942	-75.942	168	56	0	102
39	Ross Sea	165.456	-76.055	169	64	0	94
40	Ross Sea	166.368	-75.849	8	61	0	85
41	Ross Sea	164.640	-76.047	16	75	1	105
42	Ross Sea	167.204	-75.720	165	80	11	115

In this region, FID 5 (75/30) had the highest potential of reactivation for a thrust faulting stress regime (NCFR = 92), despite always being located a few hundred kilometers from the grounding line. In the Amundsen Sea, 91% of the 115 NCFR of FID 3 (150/60) are in a strike-slip faulting stress regime with $S_{Hmax} = 45^\circ$ or $S_{Hmax} = 90^\circ$. According to model IJ05_R2, instability peaked between 15 and 14 ka BP. Using model W12, instability started after 17 ka BP. Under a strike-slip faulting stress regime, FID 6 (75/60) shows instability for 88% of the 24 NCFR with $S_{Hmax} = 0^\circ/R = 0.05$.

FIDs 9, 10, and 11 are the same fault with a strike direction of 165° , but dip angles of 75° , 60° , and 45° , respectively. From the three tested dip angles, fault geometry of FID 9 is the closest to the optimal orientation in a strike-slip faulting regime for $S_{Hmax} = 45^\circ$. This FID had the highest NCFR (85) of the three tested orientations, while FID 11 had the lowest NCFR (12). All ice retreat periods were accompanied or followed by an increase in ΔCFS values for these FIDs (Figure 6).

4.3. Ross Sea

In the Ross Sea all 25 faults (FIDs 31–55) have non-zero NCFR in a strike-slip faulting stress regime (Figure 7, top). FIDs 31, 32, 33, 35, 41, and 42 also show NCFR within a thrust faulting stress regime (Figure 7, bottom). The NCFR under the former is significantly higher than the one in the latter: the highest NCFR for a thrust faulting stress regime is 21 (for FID 33), whilst in a strike-slip faulting stress regime it is 115 (for FID 42).

FIDs 43–54 are located south of the Ross Sea, in Victoria Land. The faults were obtained from the International Database of Glacially Induced Faults (Munier et al., 2020) and tested with dips of 45° , 60° , and 75° . For these faults, a larger potential of reactivation is observed for steeper dips and during periods of higher deglaciation rates in both stress regimes. The highest NCFR was for a strike-slip faulting stress regime: 84 for FIDs 46, 49, 52, and 53. In a thrust faulting stress regime the highest NCFR was 20 for FID 52. FIDs with the same geometry had similar results.

4.4. Lazarev and Weddell Seas

In the Lazarev and Weddell seas, none of the seven identified faults (FIDs 56–62) have a potential of reactivation within a thrust faulting stress regime, while six faults have a non-zero NCFR within a strike-slip faulting stress regime (Figure 8). In the Lazarev Sea, FIDs 56 (90/90, NCFR = 57), 57 (90/60, NCFR = 21) and 58 (90/60, NCFR = 21) had similar ice coverage since the LGM. FID 56 shows periods of potential reactivation during this time, while FIDs 57 and 58 have stress-model combinations showing instability since the LGM.

In the Weddell Sea, for FID 61 (0/60) all 33 NCFR show instability for $S_{Hmax} = 90^\circ/R = 0.05$, while for FID 62 (45/60) all 34 NCFR are for $S_{Hmax} = 135^\circ/R = 0.05$. FID 60 (120/75) has a NCFR of 83, showing instability for all stress ratios for $S_{Hmax} = 45^\circ$ and $S_{Hmax} = 0^\circ$.

4.5. Prydz Bay

In the Prydz Bay area 10 faults were evaluated (Figure 9; FIDs 21–30). From these, FID 23 (105/75) has the highest total NCFR (118) and is the only one which presented instability in a thrust faulting stress regime for 13 stress-model combinations. FIDs 25, 26, and 27 correspond to dip angles of 75° ,

Table 1
Continued

FID	Region	Longitude	Latitude	Strike	Dip	TF	SSF
43 ^a	Ross Sea	163.779	-78.156	43	80	0	54
44 ^a	Ross Sea	163.779	-78.156	43	65	0	35
45 ^a	Ross Sea	163.779	-78.156	43	50	1	13
46 ^a	Ross Sea	163.589	-78.133	30	80	13	84
47 ^a	Ross Sea	163.589	-78.133	30	65	2	81
48 ^a	Ross Sea	163.589	-78.133	30	50	0	12
49 ^a	Ross Sea	163.640	-78.123	30	80	13	84
50 ^a	Ross Sea	163.640	-78.123	30	65	2	83
51 ^a	Ross Sea	163.640	-78.123	30	50	0	12
52 ^a	Ross Sea	163.958	-78.027	23	80	20	84
53 ^a	Ross Sea	163.958	-78.027	23	65	2	84
54 ^a	Ross Sea	163.958	-78.027	23	50	0	15
55	Ross Sea	-169.083	-77.999	178	61	0	21
56	Lazarev Sea	10.338	-68.884	84	83	0	57
57	Lazarev Sea	10.309	-68.896	89	59	0	21
58	Lazarev Sea	-5.865	-68.857	94	62	0	21
59	Weddell Sea	-27.829	-73.067	92	33	0	0
60 ^c	Weddell Sea	-59.495	-75.057	120	81	0	83
61	Weddell Sea	-28.655	-73.720	177	63	0	33
62	Weddell Sea	-28.518	-73.772	41	60	0	34

Note. FID: Fault identification number. TF: number of combinations indicating fault reactivation (NCFR) in a thrust faulting stress regime. SSF: NCFR in a strike-slip faulting stress regime. No symbol: strike from at least two seismic profiles. ^aStrike from trend in maps and different ranges of dips. ^bStrike from trend in maps and dip from Bell and King (1998). ^cStrike from trend in maps and dip from seismic profile.

60°, and 45°, respectively, for the same fault with a strike of 165°. In a strike-slip faulting stress regime FID 25 has the highest NCFR (39) of the three FIDs. Similarly, FIDs 28, 29, and 30 have dips of 75°, 60°, and 45° with a fault strike of 150°. Of these three FIDs, FID 29 has the highest NCFR (41) and FID 30 the lowest (12).

5. Discussion

GIFs are mostly reported in northern Europe, and despite deglaciation in Fennoscandia being well researched (Stroeven et al., 2016), it is still difficult to constrain the mechanisms related to fault reactivation due to the complexity and lack of certainty of the background stress regime (R. Steffen & Steffen, 2021b; R. Steffen et al., 2014). In Antarctica, the available data regarding both deglaciation since the LGM and background stress regimes is undoubtedly scarcer. The sparse information about the ice sheet history and Earth's rheology increases the uncertainties in GIA modeling (Martín-Español et al., 2016). To accommodate these potential uncertainties, we have tested a set of 10 different 3D Earth models and two ice models. H. Steffen and Steffen (2024a) showed that the choice of the ice model affects the stress behavior more than the choice of the Earth model. Our findings support this as differences in the total NCFR between the 3D Earth models were negligible when compared to the ice models. Hence, future investigations on glacially induced stresses should be made with ice models of the next generation including ice model uncertainties.

A major component of the 3D Earth models is the difference in lithospheric thickness and mantle viscosities between East and West Antarctica. West Antarctica is dominated by a thin crust on top of a warm and weak mantle, while East Antarctica has a thick crust and stiff mantle (Martin et al., 2023; Nield et al., 2023; van Calcar et al., 2023). Despite this, noticeable differences between the number of combinations indicating reactivation of faults located in East and West Antarctica are not detected in our study. It is important to highlight, however, that 46 of the 62 identified faults are located in West Antarctica. Although this study covers a large portion of marine Antarctica, and a few continental areas, most of the continental shelf of East Antarctica

and regions of West Antarctica are not investigated due to the lack of seismic data or faulting information in these areas. We may forecast more areas with potential GIFs once data coverage allows an extended investigation.

In regard to the ice models, W12 can be considered to be more finely tuned than IJ05_R2 (Shepherd et al., 2012), with a lower overall excess in the AIS volume (relative to present) compared to IJ05_R2. Excess in AIS volume in East Antarctica could suggest model IJ05_R2 has a better fit of its ice content for Prydz Bay, although M. A. King et al. (2022) noted that both models perform similarly in this region. Since the NCFR for most faults is similar for both ice models, a robust evaluation of the potential for glacially triggered faulting in Antarctica can likely be made using either model. However, the two models are not interchangeable. Some faults show significantly different results for each and should be evaluated with caution. FID 60, for example, has a NCFR of 18 in ice model IJ05_R2, while in ice model W12, the NCFR is 65.

With respect to the tectonic setting, the dependence of the NCFR on specific stress regimes and ratios highlights the importance of knowing the background stress parameters when analysing glacially induced stresses. Our results rely on the presumption of an initially critically stressed crust, and therefore if the pre-glacial conditions of Antarctica are proven to be of a non-critically stressed crust, they might be misleading. R. Steffen and Steffen (2021b) and Walsh and Zoback (2015), however, argued that the presence of GIFs in Fennoscandia and Oklahoma, respectively, defend the existence of a critically stressed crust. The Amundsen and Bellingshausen seas are the only areas where a higher NCFR is observed in a thrust faulting stress regime. The faults identified in these regions also have geometries that are closer to optimal for this stress regime, reflecting a predictable trend: faults with an orientation closer to optimal tend to show higher instability. A similar pattern emerges when testing

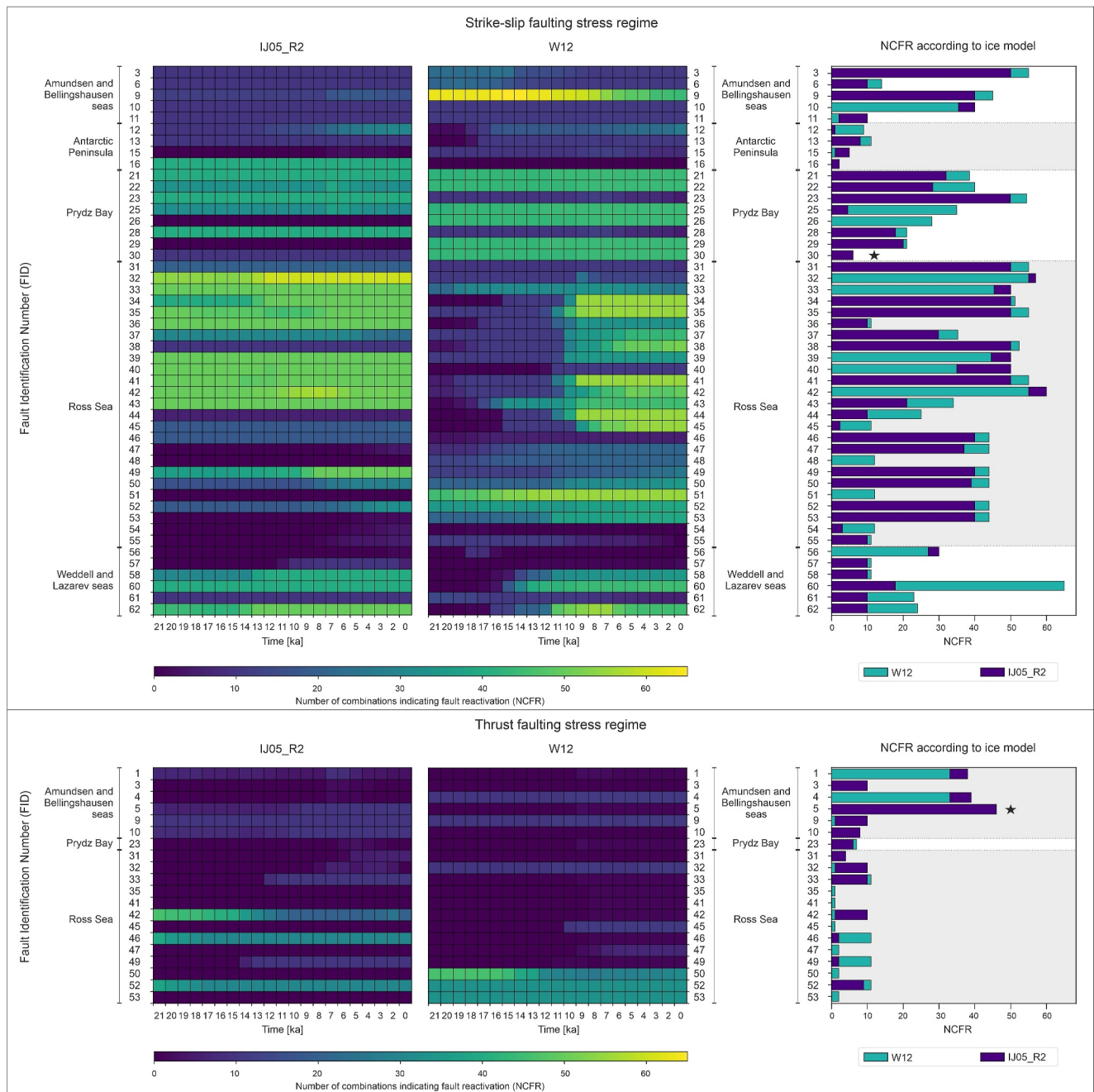


Figure 3. Number of combinations indicating fault reactivation (NCFR) for ice models IJ05_R2 and W12 in a strike-slip faulting and a thrust faulting stress regime (top and bottom, respectively). NCFR according to the time step and ice model (left) and total NCFR according to the ice model (right). Faults indicated with a star have the same value for both ice models. Location of faults indicated by name of the research area.

faults using various dip angles. A higher NCFR is observed in a strike-slip faulting regime for steeper angles, which are closer to the optimal orientation in such a stress regime. Notwithstanding, many faults in this study became unstable regardless of orientation, and research indicates glacially triggered faulting in North and Central Europe can happen even for faults with a non-optimal orientation (Lagerbäck & Sundh, 2008; R. Steffen & Steffen, 2021b).

Reactivation of non-optimal oriented faults could also be a result of stress regime changes due to the additional glacially induced stresses. Except for FIDs 1, 4, and 5 (Amundsen Sea), all faults that show instability in a thrust

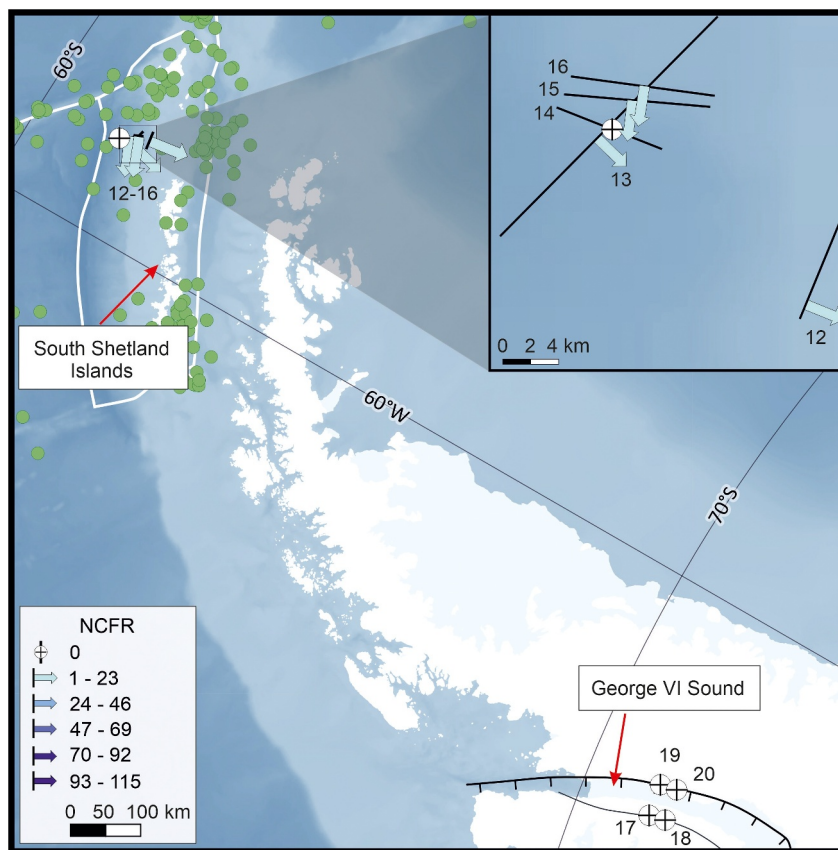


Figure 4. Number of combinations indicating fault reactivation (NCFR) in the Antarctic Peninsula region for a strike-slip faulting stress regime. In a thrust faulting stress regime all faults have a NCFR of zero. South Shetland Islands and George VI Sound indicated by red arrows. Black lines: fault trend. Railway lines: rifting (Kalberg et al., 2015). White lines: tectonic plate boundaries (Bird, 2003). Arrows: dip direction. Green dots: earthquakes of known magnitude from 1904 to 2022 according to the International Seismological Center (ISC) Bulletin.

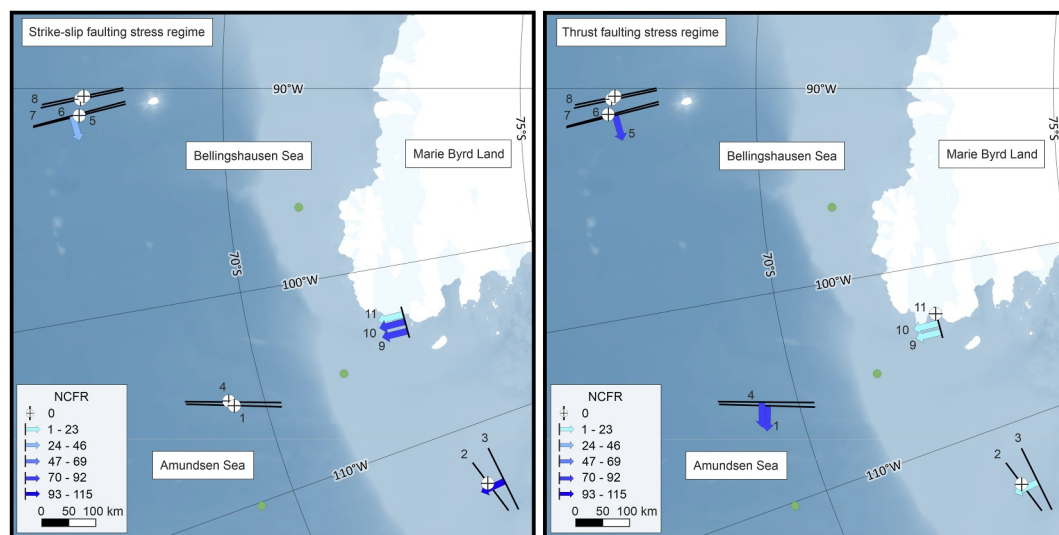


Figure 5. Number of combinations indicating fault reactivation (NCFR) in the Amundsen and Bellingshausen seas region for a strike-slip (left) and thrust faulting (right) stress regime. Black lines: fault trend. Arrows: dip direction. Green dots: earthquakes of known magnitude from 1904 to 2022 according to the International Seismological Center (ISC) Bulletin.

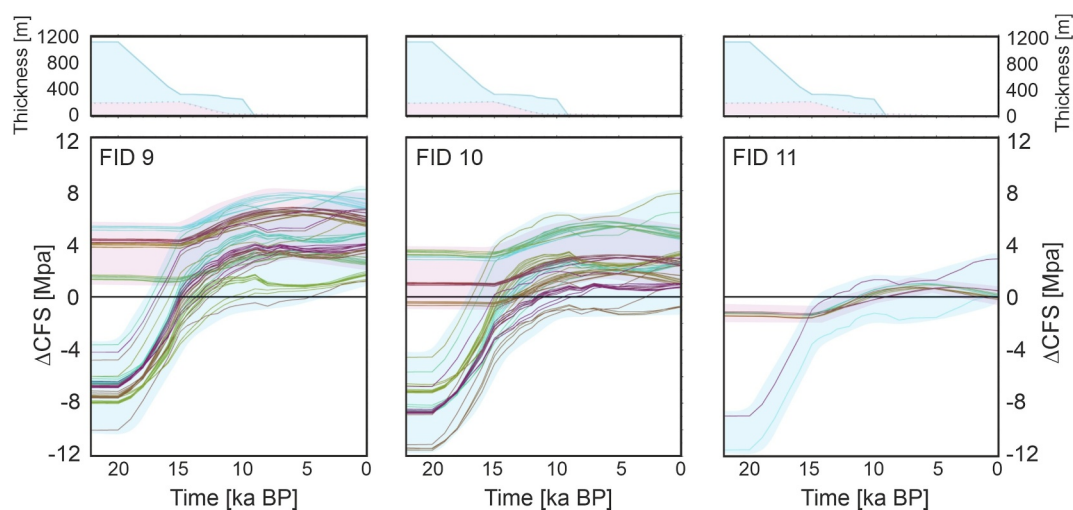


Figure 6. Change of Coulomb failure stress (ΔCFS) in the last 21,000 years for a fault with a strike of 165° tested for dips of 75° (FID 9), 60° (FID 10) and 45° (FID 11) in a strike-slip faulting stress regime. Each individual line represents the ΔCFS for one stress-model combination at each timestep. Upper plots: ice thickness for ice model W12 (blue background) and IJ05_R2 (pink background). The same color coding is used for the lower panel of ΔCFS to separate the results for the two ice models.

faulting stress regime only become unstable at high stress ratios. In contrast, higher fault instability is observed for low stress ratios within a strike-slip faulting regime. R. Steffen and Steffen (2021b) found that it is possible for a thrust fault to be reactivated in a strike-slip faulting stress regime and a strike-slip fault to be reactivated in a thrust faulting stress regime due to the similarities of the intermediate and minimum principal stress magnitudes for $R = 0.95$. Similarly, normal faults could be reactivated in a strike-slip faulting stress regime with a stress ratio R of 0.05. Thus, a small change (e.g., due to GIA) can lead to a shift in the stress regime (e.g., from a thrust faulting to strike-slip faulting stress regime). This theory could support glacially triggered faulting in a strike-slip faulting stress regime for the faults north of the Antarctic Peninsula, as they are reported to be of thrust and normal orientation by Loreto et al. (2011). These faults could have been reactivated as thrust or normal faults, despite assuming a strike-slip stress regime here. The same can also be valid for faults 43–54, observed in Victoria Land. These faults have been reported to be of strike-slip character by S. Jones (1997), and instability in a thrust faulting stress regime was solely observed for $R = 0.95$. As the area is dominated by strike-slip to normal faulting (see Section 2), it is consistent that the highest NCFR are seen in a strike-slip faulting stress regime. Our results imply that while GIFs in Antarctica are more likely to exist under stress conditions favorable to fault failure, glacially triggered faulting could also occur under non-optimal conditions.

Regional tectonics can also impact glacially triggered faulting; for example, Kreemer et al. (2018) suggested that GIFs in Northern America might be linked to anomalous stress conditions. Results from Global Navigation Satellite System (GNSS) data indicate a clockwise rotation of the Antarctic Plate, with higher horizontal velocities (Savchyn et al., 2023) and uplift rates (Sunil et al., 2022) in West Antarctica compared to East Antarctica. The overall plate motion in the Cenozoic, along with geological evidence and GNSS data, indicates a stress regime dominated by strike-slip and normal faulting components (see Section 2, Maestro et al., 2008; Zanutta et al., 2018). A strike-slip faulting stress regime is consistent with higher fault instabilities due to GIA for the Ross and Weddell seas. However, Antarctica exhibits a heterogeneous horizontal strain velocity field (Savchyn et al., 2023). West Antarctica, especially, is affected by the intricate interactions between neotectonics, volcanism and GIA, all of which may contribute to a regionally complex stress field. Deformation rates in the lithosphere are highest onshore of the Amundsen and Bellingshausen seas and in the Antarctic Peninsula, most likely due to the viscoelastic response of the Earth to ice-mass changes (Barletta et al., 2018; Nield et al., 2014). Areas of high strain rate, however, are not necessarily associated with higher seismicity in intraplate regions and might be even anticorrelated (Kreemer et al., 2018). Indeed, our results suggest below average NCFR for the Antarctic Peninsula. The Amundsen and Bellingshausen seas, however, presented high NCFR in both stress regimes, which could be a response to the complex stress field, or simply a biased result due to optimal fault orientation.

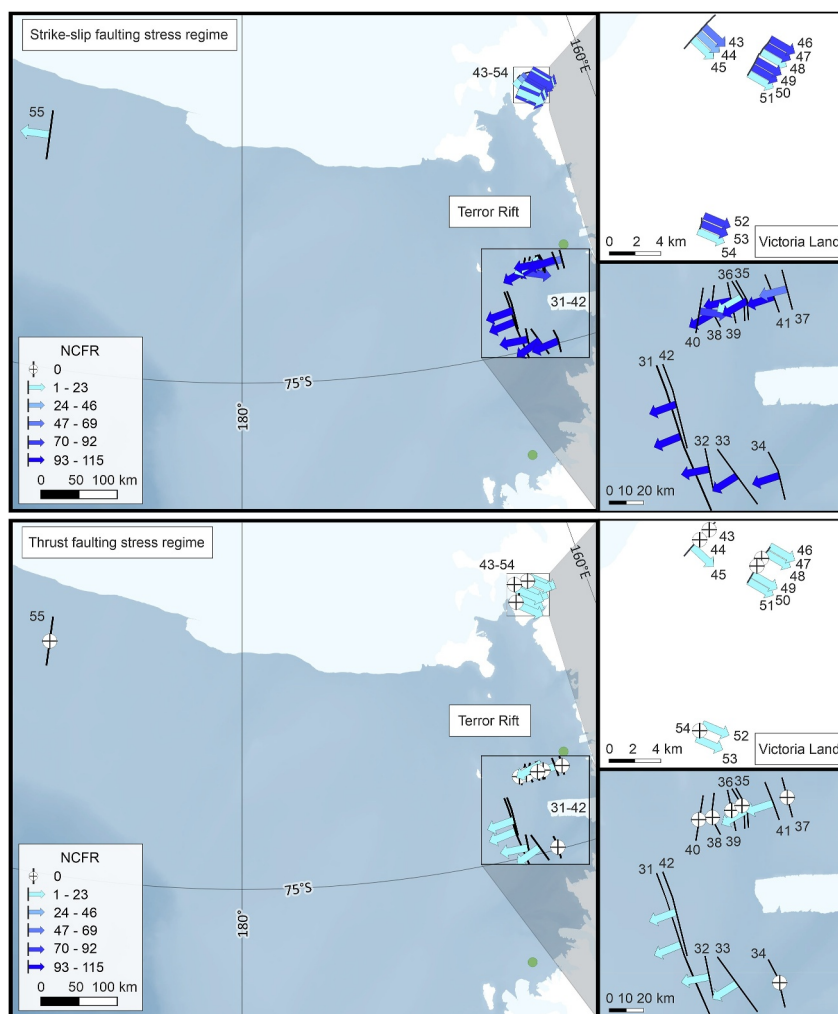


Figure 7. Number of combinations indicating fault reactivation (NCFR) in the Ross Sea region for a strike-slip (top) and thrust faulting (bottom) stress regime. Black lines: fault trend. Arrows: dip direction. Green dots: earthquakes of known magnitude from 1904 to 2022 according to the International Seismological Center (ISC) Bulletin.

The Antarctic Peninsula also differs from the other research areas: it exhibits flares of magmatism, its northern region is located in an ancient subduction zone, and the Bransfield Strait is undergoing crustal extension (e.g., Cesca et al., 2022). Moment tensor data indicate the presence of normal, thrust, and strike-slip faulting events (Ekström et al., 2012). Since the 1900s over 50 earthquakes have been reported at a radius of 100 km from the identified faults in this region (International Seismological Centre, 2024). Most of these had a depth of over 10 km, whilst in the model we use a depth of 2.5 km, where ΔCFS is calculated. However, if the area is dominated by a strike-slip to normal faulting stress regime of $S_{H\text{max}} = 135^\circ$, as reported by the World Stress Map (Heidbach et al., 2016), our results show a possibility of glacially triggered faulting in the region. In addition, the measured dip values and ΔCFS values obtained at the depth of 2.5 km might not correspond to the values obtained at greater depths (e.g., 10 km), where earthquake nucleation typically occurs. Instability due to GIA might occur for deeper parts of the faults when the dip angles become more optimally oriented in the prevailing stress regime and ΔCFS values become higher. It is reasonable to assume that the present seismicity in the Antarctic Peninsula may be driven by complex interactions between tectonic and glacial mechanisms.

GIA-induced stresses and its connection to seismicity is complex even in areas with higher data quality (e.g., Seidel et al., 2025). Grosset et al. (2023) showed that present-day seismicity in the Western Alps cannot be explained by glacially induced stresses, and they tend to either inhibit fault slip or promote deformation with the wrong mechanism compared to the observed data. Here, we observe a correlation between the ΔCFS tendencies

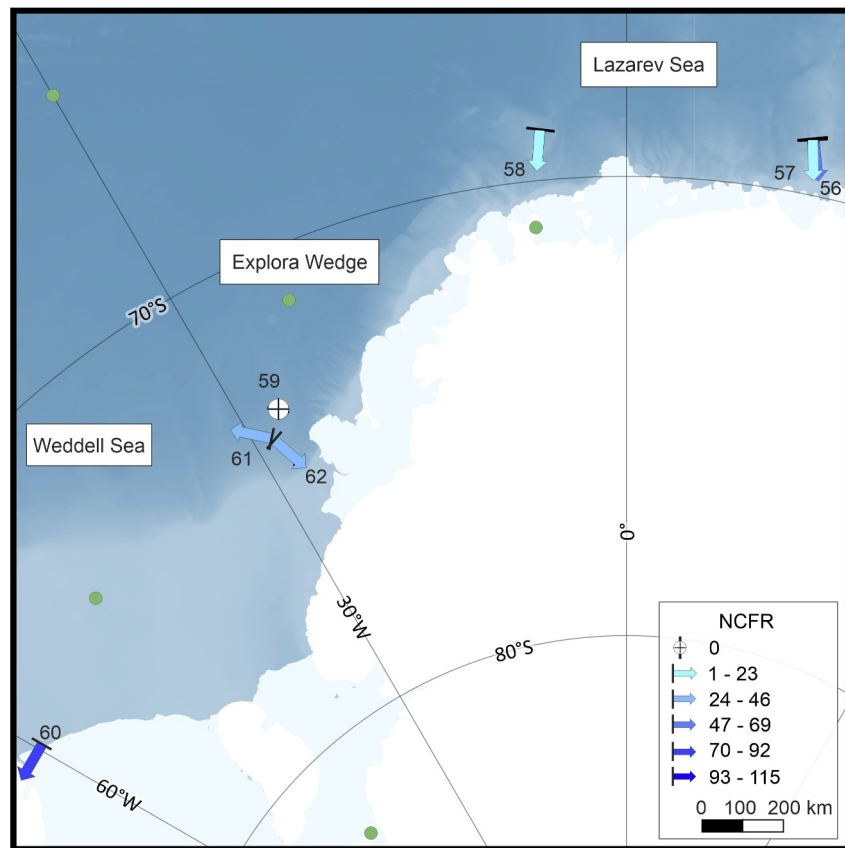


Figure 8. Number of combinations indicating fault reactivation (NCFR) in the Lazarev and Weddell seas region for a strike-slip faulting stress regime. In a thrust faulting stress regime all faults have a NCFR of zero. Black lines: fault trend. Arrows: dip direction. Green dots: earthquakes of known magnitude from 1904 to 2022 according to the International Seismological Center (ISC) Bulletin.

and the glaciation period across almost all faults, with most showing increased instability as the ice shelf receded. This was at 12 ka BP in the continental shelf of the Amundsen Sea and at Prydz Bay, between 17 and 12 ka BP in the Ross Sea and at 10 ka BP in Victoria Land, the Lazarev and Weddell seas. Despite many of these faults remaining unstable until today, the seismicity of Antarctica is still low when compared to other intraplate regions (Antonovskaya et al., 2021; Martín-González et al., 2023). One possible explanation to this could be that past earthquakes released glacially induced stresses, decreasing instability afterward, as has been suggested to have happened in Greenland during the Holocene (R. Steffen et al., 2020). Another possibility, is that earthquakes are not recorded due to low coverage of seismic networks or they are overlooked by seismological centers (Reading, 2007). Close to Balleny Islands, 330 km north of the Antarctic continental shelf, an earthquake of magnitude M_W 8.1 in 1998, has been linked to GIA and post-seismic deformation in the Antarctic plate (Kanao, 2018; Kaufmann et al., 2005; Tsuboi et al., 2000).

Lough et al. (2018) stated the seismicity rate of East Antarctica is comparable to other cratons and seismicity might be contained within ancient rift systems. The same theory had been previously raised by Reading (2007), who suggested that the Antarctic oceanic lithosphere could possibly support high stress rates due to the presence of spreading ridges (Reading, 2006). Our results show the highest NCFR in areas that have experienced rifting, noticeably the Ross, Amundsen and Bellingshausen seas. If our initial conditions are valid, these findings suggest that these areas could undergo glacially triggered faulting under a wider range of stress conditions and may potentially serve as sites for stress relief under varying stress states. With the increased deployment of seismic stations in the Antarctic in the last two decades, the number of recorded earthquakes has almost doubled when compared to the previous 100 years (International Seismological Centre, 2024). Most of these events are of low magnitude and cannot be resolved for focal mechanisms. A continued and extended station coverage is needed to

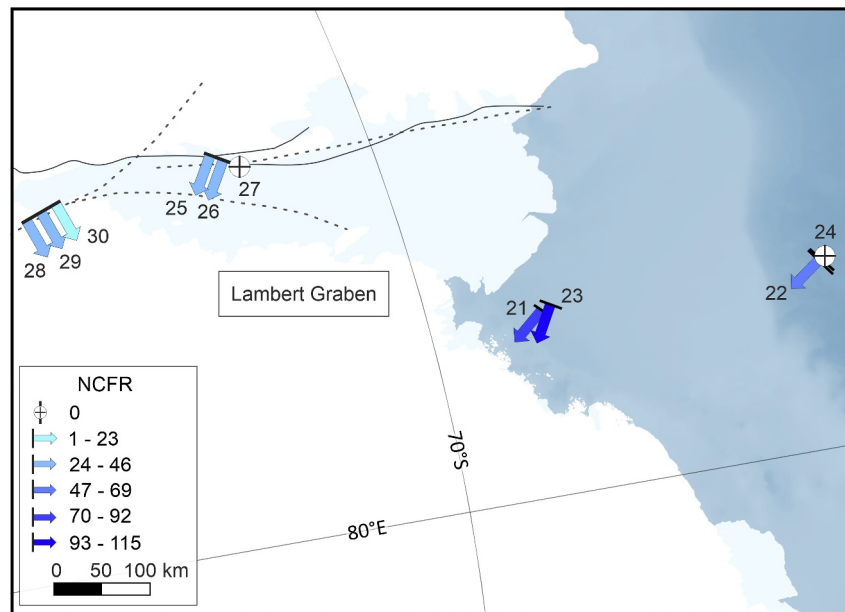


Figure 9. Number of combinations indicating fault reactivation (NCFR) in the Prydz Bay region for a strike-slip faulting stress regime. In a thrust faulting stress regime fault number 23 has a NCFR of 13 and all other faults have a NCFR of zero. Black lines: fault trend. Dashed lines: inferred faults. Arrows: dip direction. In this area there are no earthquakes of known magnitude from 1904 to 2022 according to the International Seismological Center (ISC) Bulletin.

record seismic events with higher resolution, providing valuable data for evaluating stress fields and refining rheological parameters.

To summarize, even though that the lack of high quality background stress field information combined with GIA modeling uncertainties provide difficulties in assessing the potential for glacially triggered faulting, we could show that most of the studied faults could have been reactivated by GIA since the LGM. The differences obtained in the number of combinations indicating fault reactivation caused by the glacial coverage highlight the importance of improved GIA models, in particular ice models, to investigate glacially triggered faulting in the past and to robustly predict its potential occurrence in the near future. Our research could assist in pointing to areas where GIFs are more likely to be found and areas where seismicity might be associated with other stress-relieve events.

6. Conclusions

Glacially triggered faulting in Antarctica is a little-studied research topic. Despite the generally increasing quality of GIA models, it is still difficult to assess the effects of GIA in this region due to many uncertainties regarding the stress field and the ice sheet history models. In this study, we evaluated the potential for glacially triggered faulting in Antarctica since the LGM for a strike-slip and thrust faulting stress regime presuming an initially critically stressed crust. Using a Finite Element model to calculate the glacially induced stress changes, we investigated the potential of 62 faults being reactivated through Coulomb failure stress changes.

Our modeling results show that the choice of the ice model has a greater influence on the potential for fault reactivation than the Earth models. In Antarctica glacially triggered faulting is more likely to occur under a strike-slip faulting stress regime. If it can be determined that the majority of our investigated faults was indeed reactivated due to glacially induced stresses, this might indicate a predominance of this type of stress regime throughout the region. Both optimally and non-optimally oriented faults can be reactivated by glacially induced stresses.

Faults in the Amundsen and Bellingshausen seas are more likely to be reactivated in a thrust faulting stress regime, which might be associated with a complex interaction between tectonics and GIA. In contrast, in a strike-slip faulting stress regime the potential for glacially triggered faulting increased since the LGM in times of rapid

ice retreat in the Prydz Bay, the Ross Sea, and the Lazarev Sea. In the Antarctic Peninsula, Weddell Sea and Lazarev Sea, the tested faults have no potential of reactivation in a thrust faulting stress regime.

To our knowledge, this is the first study to investigate the Circum-Antarctic potential for glacially triggered faulting. Regions of Antarctica that have experienced past rifting are potential sites of GIFs. We have shown that since the LGM, fault instability has increased for the parameters studied, with many regions remaining unstable to this day. Thus, continuous seismic station deployment is required to monitor the existence of glacially triggered faulting events.

Data Availability Statement

The seismic profiles used for identifying the faults in the study are available at the Antarctic Seismic Data Library System (2024). The International Database of Glacially Induced Faults can be obtained at Munier et al. (2020). The lithosphere thickness model is taken from Lloyd et al. (2020). The 10 global 3D viscosity models used in this research are available at R. Steffen and Steffen (2024b). The modeled Coulomb failure stress changes in the last 21,000 years for the 62 locations of the Circum-Antarctic faults can be found in H. Steffen and Steffen (2025). The GIS project used to create the maps is available at Barbosa (2024).

Acknowledgments

We are grateful to the Norwegian Polar Institute, the SCAR Antarctic Digital Database and the numerous organizations that contributed their seismic data to the SDLS. This study contributes to the research topic “Causes and Effects of Climate Change in the Earth System” of the Center for Earth System Research and Sustainability (CEN) at the University of Hamburg and to the AWI Research Program “Changing Earth—Sustaining our Future” with its Subtopic 2.1 “Warming Climates.” The study benefited from discussions during the GIA Training School 2023 at Lantmäteriet in Gävle, Sweden. We also thank Anya M. Reading, Christie Rowe, one anonymous reviewer and associate editor Augusto Rapalini for their constructive comments that helped in improving this manuscript. Finally, we thank Erik Ivins and Pippa Whitehouse for providing the ice models IJ05_R2 and W12, respectively. Open Access funding enabled and organized by Projekt DEAL.

References

- Ahmadi, O., Juhlin, C., Ask, M., & Lund, B. (2015). Revealing the deeper structure of the end-glacial Pärvie fault system in northern Sweden by seismic reflection profiling. *Solid Earth*, 6(2), 621–632. <https://doi.org/10.5194/se-6-621-2015>
- An, M., Wiens, D. A., Zhao, Y., Feng, M., Nyblade, A., Kanao, M., et al. (2015a). S-velocity model and inferred Moho topography beneath the Antarctic Plate from Rayleigh waves. *Journal of Geophysical Research: Solid Earth*, 120(1), 359–383. <https://doi.org/10.1002/2014JB011332>
- An, M., Wiens, D. A., Zhao, Y., Feng, M., Nyblade, A., Kanao, M., et al. (2015b). Temperature, lithosphere-asthenosphere boundary, and heat flux beneath the Antarctic Plate inferred from seismic velocities. *Journal of Geophysical Research: Solid Earth*, 120(12), 8720–8742. <https://doi.org/10.1002/2015JB011917>
- Anderson, J. B., Conway, H., Bart, P. J., Witus, A. E., Greenwood, S. L., McKay, R. M., et al. (2014). Ross Sea paleo-ice sheet drainage and deglacial history during and since the LGM. *Quaternary Science Reviews*, 100, 31–54. <https://doi.org/10.1016/j.quascirev.2013.08.020>
- Anderson, J. B., Shipp, S. S., Lowe, A. L., Wellner, J. S., & Mosola, A. B. (2002). The Antarctic ice sheet during the last glacial maximum and its subsequent retreat history: A review. *Quaternary Science Reviews*, 21(1–3), 49–70. [https://doi.org/10.1016/S0277-3791\(01\)00083-X](https://doi.org/10.1016/S0277-3791(01)00083-X)
- Antarctic Seismic Data Library System. (2024). Scientific Committee on Antarctic Research [Dataset]. *Antarctic Seismic Data Library System*. Retrieved from <https://sdls.ogs.trieste.it/cache/index.jsp>
- Antonovskaya, G. N., Basakina, I. M., Vaganova, N. V., Kapustian, N. K., Konechnaya, Y. V., & Morozov, A. N. (2021). Spatiotemporal relationship between Arctic mid-ocean ridge system and intraplate seismicity of the European Arctic. *Seismological Research Letters*, 92(5), 2876–2890. <https://doi.org/10.1785/0220210024>
- Argus, D. F., Peltier, W. R., Drummond, R., & Moore, A. W. (2014). The Antarctica component of postglacial rebound model ICE-6G_C (VM5a) based on GPS positioning, exposure age dating of ice thicknesses, and relative sea level histories. *Geophysical Journal International*, 198(1), 537–563. <https://doi.org/10.1093/gji/ggu140>
- Arndt, J. E., Larter, R. D., Hillenbrand, C.-D., Sørli, S. H., Forwick, M., Smith, J. A., & Wacker, L. (2020). Past ice sheet-seabed interactions in the northeastern Weddell Sea embayment, Antarctica. *The Cryosphere*, 14(6), 2115–2135. <https://doi.org/10.5194/tc-14-2115-2020>
- Bagge, M., Klemann, V., Steinberger, B., Latinović, M., & Thomas, M. (2021). Glacial-isostatic adjustment models using geodynamically constrained 3D Earth structures. *Geochemistry, Geophysics, Geosystems*, 22(11). <https://doi.org/10.1029/2021GC009853>
- Barbosa, I. (2024). The tectonic background and the potential for glacially triggered faulting of 62 faults identified in Antarctica [Dataset]. *Zenodo*. <https://doi.org/10.5281/zenodo.13942569>
- Barletta, V. R., Bevis, M., Smith, B. E., Wilson, T., Brown, A., Bordon, A., et al. (2018). Observed rapid bedrock uplift in Amundsen Sea Embayment promotes ice-sheet stability. *Science*, 360(6395), 1335–1339. <https://doi.org/10.1126/science.aao1447>
- Becker, T. W., & Boschi, L. (2002). A comparison of tomographic and geodynamic mantle models. *Geochemistry, Geophysics, Geosystems*, 3(1). <https://doi.org/10.1029/2001GC000168>
- Bell, A. C., & King, E. C. (1998). New seismic data support Cenozoic rifting in George VI Sound, Antarctic Peninsula. *Geophysical Journal International*, 134(3), 889–902. <https://doi.org/10.1046/j.1365-246X.1998.00605.x>
- Bent, A. L. (1994). The 1989 (MS 6.3) Ungava, Quebec, earthquake: A complex intraplate event. *Bulletin of the Seismological Society of America*, 84(4), 1075–1088. <https://doi.org/10.1785/BSSA0840041075>
- Bentley, M. J., Fogwill, C. J., Kubik, P. W., & Sugden, D. E. (2006). Geomorphological evidence and cosmogenic $^{10}\text{Be}/^{26}\text{Al}$ exposure ages for the last glacial maximum and deglaciation of the Antarctic Peninsula ice sheet. *Bulletin of the Geological Society of America*, 118(9–10), 1149–1159. <https://doi.org/10.1130/B25735.1>
- Bentley, M. J., Ocofaigh, C., Anderson, J. B., Conway, H., Davies, B., Graham, A. G. C., et al. (2014). A community-based geological reconstruction of Antarctic ice sheet deglaciation since the last glacial maximum. *Quaternary Science Reviews*, 100, 1–9. <https://doi.org/10.1016/j.quascirev.2014.06.025>
- Bird, P. (2003). An updated digital model of plate boundaries. *Geochemistry, Geophysics, Geosystems*, 4(3). <https://doi.org/10.1029/2001GC000252>
- Blocher, W. B. (2017). *Fault geometry and kinematics within the terror rift, Antarctica* [Master's thesis]. The Ohio State University. Retrieved from http://rave.ohiolink.edu/etdc/view?acc_num=osu1510176632279205
- Brandes, C., Steffen, H., Sandersen, P. B. E., Wu, P., & Winsemann, J. (2018). Glacially induced faulting along the NW segment of the Sorgenfrei-Tornquist Zone, northern Denmark: Implications for neotectonics and Lateglacial fault-bound basin formation. *Quaternary Science Reviews*, 189, 149–168. <https://doi.org/10.1016/j.quascirev.2018.03.036>

- Brandes, C., Steffen, H., Steffen, R., & Wu, P. (2015). Intraplate seismicity in northern Central Europe is induced by the last glaciation. *Geology*, 43(7), 611–614. <https://doi.org/10.1130/G36710.1>
- Brandes, C., Winsemann, J., Roskosch, J., Meinsen, J., Tanner, D. C., Frechen, M., et al. (2012). Activity along the Osning thrust in Central Europe during the Lateglacial: Ice-sheet and lithosphere interactions. *Quaternary Science Reviews*, 38, 49–62. <https://doi.org/10.1016/j.quascirev.2012.01.021>
- Burton-Johnson, A., & Riley, T. R. (2015). Autochthonous v. Accreted Terrane development of continental margins: A revised in situ tectonic history of the Antarctic Peninsula. *Journal of the Geological Society*, 172(6), 822–835. <https://doi.org/10.1144/jgs2014-110>
- Carson, N. J. (2012). *The Geology and geomorphology of the Denton hills, Southern Victoria Land, Antarctica* [Master's thesis]. University of Canterbury. Retrieved from <http://hdl.handle.net/10092/7467>
- Casado, M., Hébert, R., Faranda, D., & Landais, A. (2023). The quandary of detecting the signature of climate change in Antarctica. *Nature Climate Change*, 13(10), 1082–1088. <https://doi.org/10.1038/s41558-023-01791-5>
- Cesca, S., Sukan, M., Lukasz, R., Vajedian, S., Niemz, P., Plank, S., et al. (2022). Massive earthquake swarm driven by magmatic intrusion at the Bransfield Strait, Antarctica. *Communications Earth and Environment*, 3, 1–11. <https://doi.org/10.1038/s43247-022-00418-5>
- Dalziel, I. W. D., Lawver, L. A., & Murphy, J. B. (2000). Plumes, orogenesis, and supercontinental fragmentation. *Earth and Planetary Science Letters*, 178(1–2), 1–11. [https://doi.org/10.1016/S0012-821X\(00\)00061-3](https://doi.org/10.1016/S0012-821X(00)00061-3)
- Dassault Systemes. (2024). ABAQUS [Software]. *Abaqus Unified FEA*. Retrieved from <https://www.3ds.com/products-services/simulia/products/abaqus/>
- Divenere, V., Kent, D. V., & Dalziel, I. W. (1996). Summary of palaeomagnetic results from West Antarctica: Implications for the tectonic evolution of the Pacific margin of Gondwana during the Mesozoic. *Geological Society - Special Publications*, 108(1), 31–43. <https://doi.org/10.1144/GSL.SP.1996.108.01.03>
- Domack, E., O'Brien, P., Harris, P., Taylor, F., Quilty, P. G., Santis, L. D., & Raker, B. (1998). Late quaternary sediment facies in Prydz Bay, East Antarctica and their relationship to glacial advance onto the continental shelf. *Antarctic Science*, 10(3), 236–246. <https://doi.org/10.1017/s0954102098000339>
- Dziadek, R., Ferraccioli, F., & Gohl, K. (2021). High geothermal heat flow beneath Thwaites Glacier in West Antarctica inferred from aeromagnetic data. *Communications Earth and Environment*, 2(1), 162. <https://doi.org/10.1038/s43247-021-00242-3>
- Dziewoński, A. M., & Anderson, D. L. (1981). Preliminary reference earth model. *Physics of the Earth and Planetary Interiors*, 25(4), 297–356. [https://doi.org/10.1016/0031-9201\(81\)90046-7](https://doi.org/10.1016/0031-9201(81)90046-7)
- Ekström, G., Nettles, M., & Dziewoński, A. M. (2012). The global CMT project 2004–2010: Centroid-moment tensors for 13,017 earthquakes. *Physics of the Earth and Planetary Interiors*, 200, 1–9. <https://doi.org/10.1016/j.pepi.2012.04.002>
- Elliot, D. H., Fleming, T. H., Kyle, P. R., & Foland, K. A. (1999). Long-distance transport of magmas in the Jurassic Ferrar Large Igneous Province, Antarctica. *Earth and Planetary Science Letters*, 167(1–2), 89–104. [https://doi.org/10.1016/S0012-821X\(99\)00023-0](https://doi.org/10.1016/S0012-821X(99)00023-0)
- Etchecopar, A., Vasseur, G., & Daignieres, M. (1981). An inverse problem in microtectonics for the determination of stress tensors from fault striation analysis. *Journal of Structural Geology*, 3(1), 51–65. [https://doi.org/10.1016/0191-8141\(81\)90056-0](https://doi.org/10.1016/0191-8141(81)90056-0)
- Fossen, H. (2016). *Structural geology* (2nd ed.). Cambridge University Press. <https://doi.org/10.1017/9781107415096>
- Geletti, R., & Busetti, M. (2011). A double bottom simulating reflector in the western Ross Sea, Antarctica. *Journal of Geophysical Research*, 116(B4), B04101. <https://doi.org/10.1029/2010JB007864>
- Gingele, F. X., Kuhn, G., Maus, B., Melles, M., & Schöne, T. (1997). Holocene ice retreat from the Lazarev Sea shelf, East Antarctica. *Continental Shelf Research*, 17(2), 137–163. [https://doi.org/10.1016/S0278-4343\(96\)00026-X](https://doi.org/10.1016/S0278-4343(96)00026-X)
- Glasser, N. F., Davies, B. J., Carrivick, J. L., Rodés, A., Hambrey, M. J., Smellie, J. L., & Domack, E. (2014). Ice-stream initiation, duration and thinning on James Ross Island, northern Antarctic Peninsula. *Quaternary Science Reviews*, 86, 78–88. <https://doi.org/10.1016/j.quascirev.2013.11.012>
- Gohl, K., Denk, A., Eagles, G., & Wobbe, F. (2013). Deciphering tectonic phases of the Amundsen Sea Embayment shelf, West Antarctica, from a magnetic anomaly grid. *Tectonophysics*, 585, 113–123. <https://doi.org/10.1016/j.tecto.2012.06.036>
- Golledge, N. R., Fogwill, C. J., Mackintosh, A. N., & Buckley, K. M. (2012). Dynamics of the last glacial maximum Antarctic ice-sheet and its response to ocean forcing. *Proceedings of the National Academy of Sciences of the United States of America*, 109(40), 16052–16056. <https://doi.org/10.1073/pnas.1205385109>
- Grosset, J., Mazzotti, S., & Vernant, P. (2023). Glacial-isostatic-adjustment strain rate–stress paradox in the Western Alps and impact on active faults and seismicity. *Solid Earth*, 14(10), 1067–1081. <https://doi.org/10.5194/se-14-1067-2023>
- Harley, S. L., Fitzsimons, I. C. W., & Zhao, Y. (2013). Antarctica and supercontinent evolution: Historical perspectives, recent advances and unresolved issues. *Geological Society, London, Special Publications*, 383(1), 1–34. <https://doi.org/10.1144/SP383.9>
- Harris, R. A. (1998). Introduction to special section: Stress triggers, stress shadows, and implications for seismic hazard. *Journal of Geophysical Research*, 103(B10), 24347–24358. <https://doi.org/10.1029/98jb01576>
- Heath, S., Hall, B. L., Denton, G. H., Henderson, G. M., & Hendy, C. H. (2022). Ice-sheet expansion from the Ross Sea into McMurdo Sound, Antarctica, during the last two glaciations. *Quaternary Science Reviews*, 278, 107379. <https://doi.org/10.1016/j.quascirev.2022.107379>
- Heidbach, O., Rajabi, M., Cui, X., Fuchs, K., Müller, B., Reinecker, J., et al. (2018). The World Stress Map database release 2016: Crustal stress pattern across scales [Dataset]. *Tectonophysics*, 744, 484–498. <https://doi.org/10.1016/j.tecto.2018.07.007>
- Heidbach, O., Rajabi, M., Reiter, K., & Ziegler, M. (2016). World stress map database release 2016 [Dataset]. *GFZ Data Services*. <https://doi.org/10.5880/WSM.2016.001>
- Hettema, M. (2020). Analysis of mechanics of fault reactivation in depleting reservoirs. *International Journal of Rock Mechanics and Mining Sciences*, 129, 104290. <https://doi.org/10.1016/j.ijrmmms.2020.104290>
- Hillenbrand, C.-D., Bentley, M. J., Stollendorf, T. D., Hein, A. S., Kuhn, G., Graham, A. G., et al. (2014). Reconstruction of changes in the Weddell Sea sector of the Antarctic ice sheet since the last glacial maximum. *Quaternary Science Reviews*, 100, 111–136. <https://doi.org/10.1016/j.quascirev.2013.07.020>
- Hillenbrand, C.-D., Larter, R. D., Dowdeswell, J. A., Ehrmann, W., Cofaigh, C. O., Benetti, S., et al. (2010). The sedimentary legacy of a palaeo-ice stream on the shelf of the southern Bellingshausen Sea: Clues to West Antarctic glacial history during the Late Quaternary. *Quaternary Science Reviews*, 29(19–20), 2741–2763. <https://doi.org/10.1016/j.quascirev.2010.06.028>
- Hinz, K., Neben, S., Gouseva, Y. B., & Kudryavtsev, G. A. (2004). A compilation of geophysical data from the Lazarev Sea and the Riiser-Larsen Sea, Antarctica. *Marine Geophysical Researches*, 25(3–4), 233–245. <https://doi.org/10.1007/s11001-005-1319-y>
- Hodgson, D. A., Jordan, T. A., Rydt, J. D., Fretwell, P. T., Seddon, S. A., Becker, D., et al. (2019). Past and future dynamics of the Brunt Ice Shelf from seabed bathymetry and ice shelf geometry. *The Cryosphere*, 13, 545–556. <https://doi.org/10.5194/tc-13-545-2019>
- Ingólfsson, O. (2004). Quaternary glacial and climate history of Antarctica. *Developments in Quaternary Science*, 2, 3–43. [https://doi.org/10.1016/S1571-0866\(04\)80109-X](https://doi.org/10.1016/S1571-0866(04)80109-X)

- International Seismological Centre, 2024 International Seismological Centre. (2024). [On-line Bulletin]. <https://doi.org/10.31905/D808B830>
- Ivins, E. R., James, T. S., Wahr, J., Ernst, E. J., Landrer, F. W., & Simon, K. M. (2013). Antarctic contribution to sea level rise observed by GRACE with improved GIA correction. *Journal of Geophysical Research: Solid Earth*, 118(6), 3126–3141. <https://doi.org/10.1002/jgrb.50208>
- Jackson, M. G., Konter, J. G., & Becker, T. W. (2017). Primordial helium entrained by the hottest mantle plumes. *Nature*, 542(7641), 340–343. <https://doi.org/10.1038/nature21023>
- Johnston, A. C. (1987). Suppression of earthquakes by large continental ice sheets. *Nature*, 330(6147), 467–469. <https://doi.org/10.1038/330467a0>
- Jones, R. S., Johnson, J. S., Lin, Y., Mackintosh, A. N., Sefton, J. P., Smith, J. A., et al. (2022). Stability of the Antarctic ice sheet during the pre-industrial Holocene. *Nature Reviews Earth & Environment*, 3(8), 500–515. <https://doi.org/10.1038/s43017-022-00309-5>
- Jones, S. (1997). Structural inheritance from crustal anisotropy, southern Victoria Land, Antarctica. *The Antarctic Region: Geological Evolution and Processes*, 571–576.
- Jordan, T. A., Ferraccioli, F., Ross, N., Corr, H. F., Leat, P. T., Bingham, R. G., et al. (2013). Inland extent of the Weddell Sea Rift imaged by new aerogeophysical data. *Tectonophysics*, 585, 137–160. <https://doi.org/10.1016/j.tecto.2012.09.010>
- Jordan, T. A., Riley, T. R., & Siddoway, C. S. (2020). The geological history and evolution of West Antarctica. *Nature Reviews Earth & Environment*, 1(2), 117–133. <https://doi.org/10.1038/s43017-019-0013-6>
- Kalberg, T., Gohl, K., Eagles, G., & Spiegel, C. (2015). Rift processes and crustal structure of the Amundsen Sea Embayment, West Antarctica, from 3D potential field modelling. *Marine Geophysical Researches*, 36(4), 263–279. <https://doi.org/10.1007/s11001-015-9261-0>
- Kanao, M. (2018). *Studies on seismicity in the polar region*. InTech. <https://doi.org/10.5772/intechopen.78554>
- Kaufmann, G. (2004). *Program package ICEAGE, Version 2004 [Program package]*. Manuscript, Institut für Geophysik der Universität Göttingen.
- Kaufmann, G., Wu, P., & Ivins, E. R. (2005). Lateral viscosity variations beneath Antarctica and their implications on regional rebound motions and seismotectonics. *Journal of Geodynamics*, 39(2), 165–181. <https://doi.org/10.1016/j.jog.2004.08.009>
- King, G. C. P., Stein, R. S., & Lin, J. (1994). Static stress changes and the triggering of earthquakes. *Bulletin of the Seismological Society of America*, 84(3), 935–953.
- King, M. A., Watson, C. S., & White, D. (2022). GPS rates of vertical bedrock motion suggest late Holocene ice-sheet Readvance in a critical sector of East Antarctica. *Geophysical Research Letters*, 49(4). <https://doi.org/10.1029/2021GL097232>
- Klages, J. P., Kuhn, G., Hillenbrand, C.-D., Graham, A. G., Smith, J. A., Larter, R. D., et al. (2014). Retreat of the West Antarctic ice sheet from the western Amundsen Sea shelf at a pre- or early LGM stage. *Quaternary Science Reviews*, 91, 1–15. <https://doi.org/10.1016/j.quascirev.2014.02.017>
- Kreemer, C., Hammond, W. C., & Blewitt, G. (2018). A robust estimation of the 3-D intraplate deformation of the north American plate from GPS. *Journal of Geophysical Research: Solid Earth*, 123(5), 4388–4412. <https://doi.org/10.1029/2017JB015257>
- Lagerbäck, R., & Sundh, M. (2008). *Early Holocene faulting and paleoseismicity in northern Sweden* (Technical Report No. 836). Geological Survey of Sweden.
- Lamping, N., Müller, J., Esper, O., Hillenbrand, C.-D., Smith, J. A., & Kuhn, G. (2020). Highly branched isoprenoids reveal onset of deglaciation followed by dynamic sea-ice conditions in the western Amundsen Sea, Antarctica. *Quaternary Science Reviews*, 228, 106103. <https://doi.org/10.1016/j.quascirev.2019.106103>
- Larter, R. D., Anderson, J. B., Graham, A. G., Gohl, K., Hillenbrand, C.-D., Jakobsson, M., et al. (2014). Reconstruction of changes in the Amundsen Sea and Bellingshausen Sea sector of the West Antarctic ice sheet since the last glacial maximum. *Quaternary Science Reviews*, 100, 55–86. <https://doi.org/10.1016/j.quascirev.2013.10.016>
- Larter, R. D., Graham, A. G., Hillenbrand, C.-D., Smith, J. A., & Gales, J. A. (2012). Late quaternary grounded ice extent in the Filchner trough, Weddell Sea, Antarctica: New marine geophysical evidence. *Quaternary Science Reviews*, 53, 111–122. <https://doi.org/10.1016/j.quascirev.2012.08.006>
- Li, T., Wu, P., Steffen, H., & Wang, H. (2018). In search of laterally heterogeneous viscosity models of glacial isostatic adjustment with the ICE-6G C global ice history model. *Geophysical Journal International*, 214(2), 1191–1205. <https://doi.org/10.1093/GJI/GGY181>
- Li, T., Wu, P., Wang, H., Steffen, H., Khan, N. S., Engelhart, S. E., et al. (2020). Uncertainties of glacial isostatic adjustment model predictions in North America associated with 3D structure. *Geophysical Research Letters*, 47, 1–10. <https://doi.org/10.1029/2020GL087944>
- Lisker, F., Brown, R., & Fabel, D. (2003). Denudational and thermal history along a transect across the Lambert Graben, northern Prince Charles Mountains, Antarctica, derived from apatite fission track thermochronology. *Tectonics*, 22(5). <https://doi.org/10.1029/2002TC001477>
- Lloyd, A. J., Wiens, D. A., Zhu, H., Tromp, J., Nyblade, A. A., Aster, R. C., et al. (2020). Seismic structure of the Antarctic upper mantle imaged with adjoint tomography. *Journal of Geophysical Research: Solid Earth*, 125(3). <https://doi.org/10.1029/2019JB017823>
- Loreto, M. F., Tinivella, U., Accaino, F., & Giustiniani, M. (2011). Offshore Antarctic Peninsula gas hydrate reservoir characterization by geophysical data analysis. *Energies*, 4(1), 39–56. <https://doi.org/10.3390/en4010039>
- Lough, A. C., Wiens, D. A., & Nyblade, A. (2018). Reactivation of ancient Antarctic rift zones by intraplate seismicity. *Nature Geoscience*, 11(7), 515–519. <https://doi.org/10.1038/s41561-018-0140-6>
- Lund, B., Schmidt, P., & Hieronymus, C. (2009). Stress evolution and fault stability during the Weichselian glacial cycle [Technical Report]. Retrieved from <https://www.osti.gov/etdweb/biblio/971759>
- Mackintosh, A. N., Verleyen, E., O'Brien, P. E., White, D. A., Jones, R. S., McKay, R., et al. (2014). Retreat history of the East Antarctic ice sheet since the last glacial maximum. *Quaternary Science Reviews*, 100, 10–30. <https://doi.org/10.1016/j.quascirev.2013.07.024>
- Maestro, A., & López-Martínez, J. (2011). Cenozoic stress field in the southwestern Antarctic Peninsula from brittle mesostructures in Wright Peninsula, Adelaide Island. *Polish Polar Research*, 32(1), 39–58. <https://doi.org/10.2478/v10183-011-0006-8>
- Maestro, A., López-Martínez, J., Bohoyo, F., Montes, M., Nozal, F., Santillana, S., & Marensi, S. (2008). Geodynamic implications of the Cenozoic stress field on Seymour Island, West Antarctica. *Antarctic Science*, 20(2), 173–184. <https://doi.org/10.1017/S0954102007000892>
- Martin, A. P., van der Wal, W., & de Boer, B. (2023). An introduction to the geochemistry and geophysics of the Antarctic mantle. *Geological Society Memoir*, 56, 1–16. <https://doi.org/10.1144/M56-2022-21>
- Martín-Español, A., King, M. A., Zammit-Mangion, A., Andrews, S. B., Moore, P., & Bamber, J. L. (2016). An assessment of forward and inverse GIA solutions for Antarctica. *Journal of Geophysical Research: Solid Earth*, 121(9), 6947–6965. <https://doi.org/10.1002/2016JB013154>
- Martín-González, F., Crespo-Martín, C., Cesca, S., & González-Muñoz, S. (2023). Understanding seismicity and seismotectonics in a stable continental region (NW Iberian Peninsula): Implications for the nature of intraplate seismicity. *Global and Planetary Change*, 227, 104177. <https://doi.org/10.1016/j.gloplacha.2023.104177>
- Milne, G. A., Mitrovica, J. X., & Forte, A. M. (1998). The sensitivity of glacial isostatic adjustment predictions to a low-viscosity layer at the base of the upper mantle. *Earth and Planetary Science Letters*, 154(1–4), 265–278. [https://doi.org/10.1016/S0012-821X\(97\)00191-X](https://doi.org/10.1016/S0012-821X(97)00191-X)

- Mooney, W. D., Prodehl, C., & Pavlenkova, N. I. (2002). 54 Seismic velocity structure of the continental lithosphere from controlled source data. *International Geophysics*, 81, 887–910. [https://doi.org/10.1016/S0074-6142\(02\)80261-3](https://doi.org/10.1016/S0074-6142(02)80261-3)
- Müller, K., Winsemann, J., Tanner, D. C., Lege, T., Spies, T., & Brandes, C. (2021). *Glacially induced faults in Germany* (pp. 283–303). Cambridge University Press. <https://doi.org/10.1017/9781108779906.021>
- Munier, R., Adams, J., Brandes, C., Brooks, G., Dehls, J., Einarsson, P., et al. (2020). International database of glacially induced faults [Dataset]. PANGAEA. <https://doi.org/10.1594/PANGAEA.922705>
- Nichols, K. A., Goehring, B. M., Balco, G., Johnson, J. S., Hein, A. S., & Todd, C. (2019). New last glacial maximum ice thickness constraints for the Weddell Sea embayment, Antarctica. *The Cryosphere*, 13(11), 2935–2951. <https://doi.org/10.5194/tc-13-2935-2019>
- Nicolas, J. P., & Bromwich, D. H. (2014). New reconstruction of Antarctic near-surface temperatures: Multidecadal trends and reliability of global reanalyses. *Journal of Climate*, 27(21), 8070–8093. <https://doi.org/10.1175/JCLI-D-13-00733.1>
- Nield, G. A., Barletta, V. R., Bordoni, A., King, M. A., Whitehouse, P. L., Clarke, P. J., et al. (2014). Rapid bedrock uplift in the Antarctic Peninsula explained by viscoelastic response to recent ice unloading. *Earth and Planetary Science Letters*, 397, 32–41. <https://doi.org/10.1016/j.epsl.2014.04.019>
- Nield, G. A., King, M. A., Koulali, A., & Samrat, N. (2023). Postseismic deformation in the northern Antarctic Peninsula following the 2003 and 2013 Scotia Sea earthquakes. *Journal of Geophysical Research: Solid Earth*, 128(10). <https://doi.org/10.1029/2023JB026685>
- Nield, G. A., Whitehouse, P. L., van der Wal, W., Blank, B., O'Donnell, J. P., & Stuart, G. W. (2018). The impact of lateral variations in lithospheric thickness on glacial isostatic adjustment in West Antarctica. *Geophysical Journal International*, 214(2), 811–824. <https://doi.org/10.1093/gji/ggy158>
- O'Brien, P. E., Santis, L. D., Harris, P. T., Domack, E., & Quilty, P. G. (1999). Ice shelf grounding zone features of Western Prydz Bay, Antarctica: Sedimentary processes from seismic and sidescan images. *Antarctic Science*, 11(1), 78–91. <https://doi.org/10.1017/s0954102099000115>
- Okuno, J., & Miura, H. (2013). Last deglacial relative sea level variations in Antarctica derived from glacial isostatic adjustment modelling. *Geoscience Frontiers*, 4(6), 623–632. <https://doi.org/10.1016/j.gsf.2012.11.004>
- Olesen, O., Henkel, H., Lile, O. B., Mairing, E., & Rønning, J. S. (1992). Geophysical investigations of the Stuoragurra postglacial fault, Finnmark, northern Norway. *Journal of Applied Geophysics*, 29(2), 95–118. [https://doi.org/10.1016/0926-9851\(92\)90001-2](https://doi.org/10.1016/0926-9851(92)90001-2)
- Peltier, W. R. (1974). The impulse response of a Maxwell Earth. *Reviews of Geophysics*, 12(4), 649–669. <https://doi.org/10.1029/RG012i004p00649>
- Peltier, W. R. (2004). Global glacial isostasy and the surface of the ice-age earth: The ICE-5G (VM2) model and GRACE. *Annual Review of Earth and Planetary Sciences*, 32(1), 111–149. <https://doi.org/10.1146/annurev.earth.32.082503.144359>
- Phartiyal, B., Sharma, A., & Bera, S. K. (2011). Glacial lakes and geomorphological evolution of Schirmacher Oasis, East Antarctica, during late quaternary. *Quaternary International*, 235(1–2), 128–136. <https://doi.org/10.1016/j.quaint.2010.11.025>
- Pisarska-Jamrózy, M., Belzyt, S., Börner, A., Hoffmann, G., Hüneke, H., Kenzler, M., et al. (2019). The sea cliff at Dwasieden: Soft-sediment deformation structures triggered by glacial isostatic adjustment in front of the advancing Scandinavian ice sheet. *DEUQUA Special Publications*, 2, 61–67. <https://doi.org/10.5194/deuquasp-2-61-2019>
- Pisarska-Jamrózy, M., Belzyt, S., Börner, A., Hoffmann, G., Kenzler, M., Rother, H., et al. (2022). Late Pleistocene earthquakes imprinted on glaciolacustrine sediments on Gnitiz Peninsula (Usedom Island, NE Germany). *Quaternary Science Reviews*, 296, 107807. <https://doi.org/10.1016/j.quascirev.2022.107807>
- Powell, E., Latychev, K., Gomez, N., & Mitrovica, J. X. (2022). The robustness of geodetically derived 1-D Antarctic viscosity models in the presence of complex 3-D viscoelastic Earth structure. *Geophysical Journal International*, 231(1), 118–128. <https://doi.org/10.1093/gji/ggac129>
- Qin, Y., Chen, X., Carpenter, B. M., & Kolawole, F. (2018). Coulomb stress transfer influences fault reactivation in areas of wastewater injection. *Geophysical Research Letters*, 45(20), 11059–11067. <https://doi.org/10.1029/2018GL079713>
- Reading, A. M. (2006). On seismic strain-release within the Antarctic Plate. In D. K. Fütterer, D. Damaske, G. Kleinschmidt, H. Miller, & F. Tessensohn (Eds.), *Antarctica: Contributions to global earth sciences* (pp. 351–355). Springer Berlin Heidelberg. https://doi.org/10.1007/3-540-32934-X_43
- Reading, A. M. (2007). The seismicity of the Antarctic plate. *Special Papers - Geological Society of America*, 425(18), 285–298. <https://doi.org/10.1130/2007.2425>
- Reches, Z. (1987). Determination of the tectonic stress tensor from slip along faults that obey the Coulomb yield condition. *Tectonics*, 6, 849–861. <https://doi.org/10.1029/TC006i006p00849>
- Rhee, H.-H., Seong, Y.-B., Woo, J.-S., Oh, C., & Yu, B.-Y. (2022). Reconstructing the post-LGM deglacial history of Hollingsworth Glacier on Ricker Hills, Transantarctic Mountains, Antarctica. *Journal of Mountain Science*, 19(5), 1217–1230. <https://doi.org/10.1007/s11629-022-7338-1>
- Ritsema, J., Deuss, A., van Heijst, H. J., & Woodhouse, J. H. (2011). S40RTS: A degree-40 shear-velocity model for the mantle from new Rayleigh wave dispersion, teleseismic traveltimes and normal-mode splitting function measurements. *Geophysical Journal International*, 184(3), 1223–1236. <https://doi.org/10.1111/j.1365-246X.2010.04884.x>
- Rocchi, S., Storti, F., Vincenzo, G. D., & Rossetti, F. (2003). Intraplate strike-slip tectonics as an alternative to mantle plume activity for the Cenozoic rift magmatism in the Ross Sea region, Antarctica. *Geological Society - Special Publications*, 210, 145–158. <https://doi.org/10.1144/GSL.SP.2003.210.01.09>
- Salvini, F., Brancolini, G., Busetti, M., Storti, F., Mazzarini, F., & Coren, F. (1997). Cenozoic geodynamics of the Ross Sea region, Antarctica: Crustal extension, intraplate strike-slip faulting, and tectonic inheritance. *Journal of Geophysical Research*, 102(B11), 24669–24696. <https://doi.org/10.1029/97jb01643>
- Sauli, C., Sorlien, C., Busetti, M., Santis, L. D., Geletti, R., Wardell, N., & Luyendyk, B. P. (2021). Neogene development of the terror rift, western Ross Sea, Antarctica. *Geochemistry, Geophysics, Geosystems*, 22(3). <https://doi.org/10.1029/2020GC009076>
- Savchyn, I., Brusak, I., & Tretyak, K. (2023). Analysis of recent Antarctic plate kinematics based on GNSS data. *Geodesy and Geodynamics*, 14(2), 99–110. <https://doi.org/10.1016/j.geog.2022.08.004>
- Scholz, C. H. (2019). *The mechanics of earthquakes and faulting* (3rd ed.). Cambridge University Press. <https://doi.org/10.1017/9781316681473>
- Schroeder, D. M., Dowdeswell, J. A., Siegert, M. J., Bingham, R. G., Chu, W., MacKie, E. J., et al. (2019). Multidecadal observations of the Antarctic ice sheet from restored analog radar records. *Proceedings of the National Academy of Sciences of the United States of America*, 116(38), 18867–18873. <https://doi.org/10.1073/pnas.1821646116>
- Seidel, E., Steffen, H., Steffen, R., Ahlrichs, N., & Hübscher, C. (2025). Drivers of glacially induced fault reactivation in the Baltic Sea sector of the tornquist fan. *Boreas*, 54(2), 220–245. <https://doi.org/10.1111/bor.12689>

- Shepherd, A., Ivins, E. R., Geruo, A., Barletta, V. R., Bentley, M. J., Bettadpur, S., et al. (2012). A reconciled estimate of ice-sheet mass balance. *Science*, 338(6111), 1183–1189. <https://doi.org/10.1126/science.1228102>
- Sibson, R. H. (1985). A note on fault reactivation. *Journal of Structural Geology*, 7(6), 751–754. [https://doi.org/10.1016/0191-8141\(85\)90150-6](https://doi.org/10.1016/0191-8141(85)90150-6)
- Sibson, R. H. (1990). Rupture nucleation on unfavourably oriented faults. *Bulletin of the Seismological Society of America*, 80, 1580–1604.
- Siegert, M. J., Kingslake, J., Ross, N., Whitehouse, P. L., Woodward, J., Jamieson, S. S., et al. (2019). Major ice sheet change in the Weddell Sea sector of West Antarctica over the last 5,000 years. *Reviews of Geophysics*, 57(4), 1197–1223. <https://doi.org/10.1029/2019RG000651>
- Simmons, N. A., Forte, A. M., Boschi, L., & Grand, S. P. (2010). GyPSuM: A joint tomographic model of mantle density and seismic wave speeds. *Journal of Geophysical Research*, 115(B12), B12310. <https://doi.org/10.1029/2010JB007631>
- Smith, J. A., Hillenbrand, C.-D., Kuhn, G., Larter, R. D., Graham, A. G., Ehrmann, W., et al. (2011). Deglacial history of the West Antarctic ice sheet in the western Amundsen Sea embayment. *Quaternary Science Reviews*, 30(5–6), 488–505. <https://doi.org/10.1016/j.quascirev.2010.11.020>
- S&P Global. (2024). Kingdom [Software]. *S&P Global*. Retrieved from <https://kingdom.ihs.com/>
- Stagg, H. M. J. (1985). The structure and origin of Prydz Bay and MacRobertson shelf, East Antarctica. *Tectonophysics*, 114(1–4), 315–340. [https://doi.org/10.1016/0040-1951\(85\)90019-8](https://doi.org/10.1016/0040-1951(85)90019-8)
- Steffen, H., Olesen, O., & Sutinen, R. (2021). Glacially triggered faulting: A historical overview and recent developments. In H. Steffen, O. Olesen, & R. Sutinen (Eds.), *Glacially-triggered faulting* (1st ed., pp. 3–19). Cambridge University Press. <https://doi.org/10.1017/9781108779906.003>
- Steffen, H., & Steffen, R. (2021a). Indications on glacially triggered faulting in polar areas. In H. Steffen, O. Olesen, & R. Sutinen (Eds.), *Glacially-triggered faulting* (pp. 366–380). Cambridge University Press. <https://doi.org/10.1017/9781108779906.027>
- Steffen, H., & Steffen, R. (2024a). Temporal behavior of glacially induced stresses and strains at potential sites for long-term storage of used nuclear fuel in Canada. *Journal of Geophysical Research: Earth Surface*, 129(9). <https://doi.org/10.1029/2024JF007705>
- Steffen, H., & Steffen, R. (2025). Modelled Coulomb failure stress changes for 62 locations of circum-Antarctic faults since the last glacial maximum [Dataset]. *Zenodo*. <https://doi.org/10.5281/zenodo.13908574>
- Steffen, H., Steffen, R., & Tarasov, L. (2019). Modelling of glacially-induced stress changes in Latvia, Lithuania and the Kaliningrad district of Russia. *Baltica*, 32(1), 78–90. <https://doi.org/10.5200/baltica.2019.1.7>
- Steffen, R., & Steffen, H. (2021b). Reactivation of non-optimally orientated faults due to glacially induced stresses. *Tectonics*, 40(11). <https://doi.org/10.1029/2021TC006853>
- Steffen, R., & Steffen, H. (2024b). A set of global three-dimensional viscosity models based on the SMEAN2 shear-wave velocity tomography model [Dataset]. *Zenodo*. <https://doi.org/10.5281/zenodo.13907989>
- Steffen, R., Steffen, H., Weiss, R., Lecavalier, B. S., Milne, G. A., Woodroffe, S. A., & Bennike, O. (2020). Early Holocene Greenland-ice mass loss likely triggered earthquakes and tsunamis. *Earth and Planetary Science Letters*, 546, 116443. <https://doi.org/10.1016/j.epsl.2020.116443>
- Steffen, R., Steffen, H., Wu, P., & Eaton, D. W. (2014). Stress and fault parameters affecting fault slip magnitude and activation time during a glacial cycle. *Tectonics*, 33(7), 1461–1476. <https://doi.org/10.1002/2013TC003450>
- Steffen, R., Wu, P., & Lund, B. (2021). Geomechanics of glacially triggered faulting. In H. Steffen, O. Olesen, & R. Sutinen (Eds.), *Glacially-triggered faulting* (1st ed., pp. 20–39). Cambridge University Press. <https://doi.org/10.1017/9781108779906.004>
- Stein, R. (1999). Role of static stress transfer in earthquake occurrence. *Nature*, 402(6762), 605–609. <https://doi.org/10.1038/45144>
- Štěpančíková, P., Rockwell, T. K., Stemberk, J., Rhodes, E. J., Hartvich, F., Luttrell, K., et al. (2022). Acceleration of Late Pleistocene activity of a Central European fault driven by ice loading. *Earth and Planetary Science Letters*, 591, 117596. <https://doi.org/10.1016/j.epsl.2022.117596>
- Storey, B. C., & Granot, R. (2021). Tectonic history of Antarctica over the past 200 million years. *Geological Society of London*, 55(1), 9–17. <https://doi.org/10.1144/M55-2018-38>
- Storey, B. C., Leat, P., Weaver, S., Pankhurst, R., Bradshaw, J., & Kelley, S. (1999). Mantle plumes and Antarctica-New Zealand rifting: Evidence from mid-Cretaceous mafic dykes. *Journal of the Geological Society*, 156(4), 659–671. <https://doi.org/10.1144/gsjgs.156.4.0659>
- Stroeven, A. P., Hättestrand, C., Kleman, J., Heyman, J., Fabel, D., Fredin, O., et al. (2016). Deglaciation of Fennoscandia. *Quaternary Science Reviews*, 147, 91–121. <https://doi.org/10.1016/j.quascirev.2015.09.016>
- Sunil, P. S., Saji, A. P., Kumar, K. V., Ponraj, M., Amirtharaj, S., & Dhar, A. (2022). Revealing the contemporary kinematics of Antarctic plate using GPS and grace data. In N. Khare (Ed.), *Assessing the Antarctic environment from a climate change perspective: An integrated approach* (pp. 343–359). Springer International Publishing. https://doi.org/10.1007/978-3-030-87078-2_18
- Tigheelaar, M., Timmermann, A., Friedrich, T., Heinemann, M., & Pollard, D. (2019). Nonlinear response of the Antarctic Ice Sheet to late Quaternary sea level and climate forcing. *The Cryosphere*, 13(10), 2615–2631. <https://doi.org/10.5194/tc-13-2615-2019>
- Tochilin, C. J., Reiners, P. W., Thomson, S. N., Gehrels, G. E., Hemming, S. R., & Pierce, E. L. (2012). Erosional history of the Prydz Bay sector of East Antarctica from detrital apatite and zircon geo- and thermochronology multidating. *Geochemistry, Geophysics, Geosystems*, 13(11). <https://doi.org/10.1029/2012GC004364>
- Tsuboi, S., Kikuchi, M., Yamanaka, Y., & Kanao, M. (2000). The March 25, 1998 Antarctic Earthquake: Great earthquake caused by postglacial rebound. *Earth Planets and Space*, 52(2), 133–136. <https://doi.org/10.1186/BF03351621>
- Twiss, R. J., & Moores, E. M. (2007). *Structural geology* (2nd ed.). W. H. Freeman. <https://doi.org/10.1017/S0016756808004627>
- van Calcar, C. J., van de Wal, R. S. W., Blank, B., de Boer, B., & van der Wal, W. (2023). Simulation of a fully coupled 3D glacial isostatic adjustment—Ice sheet model for the Antarctic ice sheet over a glacial cycle. *Geoscientific Model Development*, 16(18), 5473–5492. <https://doi.org/10.5194/gmd-16-5473-2023>
- van der Wal, W., Barletta, V., Nield, G., & van Calcar, C. (2023). Glacial isostatic adjustment and post-seismic deformation in Antarctica. *Geological Society Memoir*, 56(1), 315–341. <https://doi.org/10.1144/M56-2022-13>
- Walsh, F. R., & Zoback, M. D. (2015). Oklahoma's recent earthquakes and saltwater disposal. *Science Advances*, 1(5). <https://doi.org/10.1126/sciadv.1500195>
- Watcham, E. P., Bentley, M. J., Hodgson, D. A., Roberts, S. J., Fretwell, P. T., Lloyd, J. M., et al. (2011). A new Holocene relative sea level curve for the South Shetland Islands, Antarctica. *Quaternary Science Reviews*, 30(21–22), 3152–3170. <https://doi.org/10.1016/j.quascirev.2011.07.021>
- White, D. A., Fink, D., Lilly, K., O'Brien, P., Dorschel, B., Berg, S., et al. (2022). Rapid ice sheet response to deglacial and Holocene paleo-environmental changes in eastern Prydz Bay, East Antarctica. *Quaternary Science Reviews*, 280, 107401. <https://doi.org/10.1016/j.quascirev.2022.107401>
- Whitehouse, P. L., Bentley, M. J., Milne, G. A., King, M. A., & Thomas, I. D. (2012). A new glacial isostatic adjustment model for Antarctica: Calibrated and tested using observations of relative sea-level change and present-day uplift rates. *Geophysical Journal International*, 190(3), 1464–1482. <https://doi.org/10.1111/j.1365-246X.2012.05557.x>

- Whitehouse, P. L., Gomez, N., King, M. A., & Wiens, D. A. (2019). Solid Earth change and the evolution of the Antarctic ice sheet. *Nature Communications*, *10*, 1–14. <https://doi.org/10.1038/s41467-018-08068-y>
- Wilson, T. J., & Paulsen, T. S. (2001). Fault and fracture patterns in CRP-3 core, Victoria Land basin, Antarctica. *Terra Antarctica*, *8*, 177–196. Retrieved from <https://core.ac.uk/outputs/11770296/>
- Wonik, T., Grelle, T., Handwerker, D., Jarrard, R., McKee, A., Patterson, T., et al. (2008). Downhole measurements in the AND-2A Borehole, ANDRILL southern McMurdo Sound project, Antarctica. *Terra Antarctica*, *15*. Retrieved from <https://digitalcommons.unl.edu/andrilrespub/47/>
- Wu, P., & Peltier, W. R. (1982). Viscous gravitational relaxation. *Geophysical Journal International*, *70*(2), 435–485. <https://doi.org/10.1111/j.1365-246X.1982.tb04976.x>
- Wu, P., Steffen, R., Steffen, H., & Lund, B. (2021). Glacial isostatic adjustment models for earthquake triggering. In *Glacially-triggered faulting* (pp. 383–401). Cambridge University Press. <https://doi.org/10.1017/9781108779906.029>
- Wu, P., Wang, H., & Steffen, H. (2013). The role of thermal effect on mantle seismic anomalies under Laurentia and Fennoscandia from observations of Glacial Isostatic Adjustment. *Geophysical Journal International*, *192*(1), 7–17. <https://doi.org/10.1093/gji/ggs009>
- Zanutta, A., Negusini, M., Vittuari, L., Martelli, L., Cianfarra, P., Salvini, F., et al. (2018). New geodetic and gravimetric maps to infer geodynamics of Antarctica with insights on Victoria Land. *Remote Sensing*, *10*, 1608. <https://doi.org/10.3390/rs10101608>
- Zoback, M. D., & Townend, J. (2001). Implications of hydrostatic pore pressures and high crustal strength for the deformation of intraplate lithosphere. *Tectonophysics*, *336*(1–4), 19–30. [https://doi.org/10.1016/S0040-1951\(01\)00091-9](https://doi.org/10.1016/S0040-1951(01)00091-9)
- Zoback, M. L., & Zoback, M. D. (2007). 6.06—Lithosphere stress and deformation. *Treatise on Geophysics*, *1–10*(1–10), 253–273. <https://doi.org/10.1016/B978-0-444-52748-6.00105-X>

References From the Supporting Information

- Amante, C., & Eakins, B. W. (2009). *Etopo1 arc-minute global relief model: Procedures, data sources and analysis*. National Geophysical Data Center. Retrieved from <https://repository.library.noaa.gov/view/noaa/1163>
- Anderson, E. M. (1951). *The dynamics of faulting and Dyke formation with application to Britain*. Oliver and Boyd.
- Arndt, J. E., Schenke, H. W., Jakobsson, M., Nitsche, F.-O., Buys, G., Goleby, B., et al. (2013). The international bathymetric chart of the southern ocean (IBCSO)—Digital bathymetric model [Dataset]. (In supplement to: Arndt, J. E. et al. (2013): The International Bathymetric Chart of the Southern Ocean Version 1.0—A new bathymetric compilation covering circum-Antarctic waters. *Geophysical Research Letters*, *40*(9), 1–7). PANGAEA. <https://doi.org/10.1594/PANGAEA.805734>
- Barker, D. H. N., & Austin, J. A. (1998). Rift propagation, detachment faulting, and associated magmatism in Bransfield Strait, Antarctic Peninsula. *Journal of Geophysical Research*, *103*(B10), 24017–24043. <https://doi.org/10.1029/98jb01117>
- Cochran, J. R., Tinto, K. J., & Bell, R. E. (2015). Abbot ice shelf, structure of the Amundsen Sea continental margin and the southern boundary of the Bellingshausen plate seaward of West Antarctica. *Geochemistry, Geophysics, Geosystems*, *16*(5), 1421–1438. <https://doi.org/10.1002/2014GC005570>
- Constantino, R. R., Tinto, K. J., Bell, R. E., Porter, D. F., & Jordan, T. A. (2020). Seafloor depth of george VI sound, Antarctic Peninsula, from inversion of aerogravity data. *Geophysical Research Letters*, *47*(21). <https://doi.org/10.1029/2020GL088654>
- Gohl, K., Teterin, D., Eagles, G., Netzeband, G., Grobys, J. W. G., Parsiegl, N., et al. (2007). *Geophysical survey reveals tectonic structures in the Amundsen Sea embayment, West Antarctica*. Geological Survey and The National Academies. <https://doi.org/10.3133/of2007-1047.srp047>
- Gohl, K. (2012). Basement control on past ice sheet dynamics in the Amundsen Sea Embayment, West Antarctica. *Palaeogeography, Palaeoclimatology, Palaeoecology*, *335–336*, 35–41. <https://doi.org/10.1016/j.palaeo.2011.02.022>
- Golynsky, D., & Golynsky, A. (2007). *Gaussberg Rift—Illusion or reality?* (pp. 1–5). U.S. Geological Survey and The National Academies. Retrieved from <https://api.semanticscholar.org/CorpusID:208958136>
- Harrowfield, M., Holdgate, G. R., Wilson, C. J., & McLoughlin, S. (2005). Tectonic significance of the Lambert graben, East Antarctica: Reconstructing the Gondwanan rift. *Geology*, *33*(3), 197–200. <https://doi.org/10.1130/G21081.1>
- Hochmuth, K., & Gohl, K. (2019). Seaward growth of Antarctic continental shelves since establishment of a continent-wide ice sheet: Patterns and mechanisms. *Palaeogeography, Palaeoclimatology, Palaeoecology*, *520*, 44–54. <https://doi.org/10.1016/j.palaeo.2019.01.025>
- Huang, X., Bernhardt, A., Santis, L. D., Wu, S., Leitchenkov, G., Harris, P., & O'Brien, P. (2020). Depositional and erosional signatures in sedimentary successions on the continental slope and rise off Prydz Bay, East Antarctica—implications for Pliocene paleoclimate. *Marine Geology*, *430*, 106339. <https://doi.org/10.1016/j.margeo.2020.106339>
- Huang, X., & Jokat, W. (2016). Sedimentation and potential venting on the rifted continental margin of Dronning Maud Land. *Marine Geophysical Researches*, *37*(4), 313–324. <https://doi.org/10.1007/s11001-016-9296-x>
- Hübscher, C. (1994). Crustal structures and location of the continental margin in the Weddell Sea/Antarctica. *Berichte zur Polarforschung*, *252*. https://doi.org/10.2312/BzP_0147_1994
- Jordan, T. A., Ferraccioli, F., & Leat, P. T. (2017). New geophysical compilations link crustal block motion to Jurassic extension and strike-slip faulting in the Weddell Sea Rift System of West Antarctica. *Gondwana Research*, *42*, 29–48. <https://doi.org/10.1016/j.gr.2016.09.009732>
- Kavoun, M., & Vinnikovskaya, O. (1994). Seismic stratigraphy and tectonics of the northwestern Weddell Sea (Antarctica) inferred from marine geophysical surveys. *Tectonophysics*, *240*(1), 299–341. [https://doi.org/10.1016/0040-1951\(94\)90277-1](https://doi.org/10.1016/0040-1951(94)90277-1)
- King, E. C., & Bell, A. C. (1996). New seismic data from the Ronne ice shelf, Antarctica. *Geological Society, London, Special Publications*, *108*(1), 213–226. <https://doi.org/10.1144/GSL.SP.1996.108.01.16>
- King, E. C., Livermore, R. A., & Storey, B. C. (1996). Weddell Sea tectonics and Gondwana break-up: An introduction. *Geological Society - Special Publications*, *108*, 1–10. <https://doi.org/10.1144/GSL.SP.1996.108.01.01>
- Leitchenkov, G. L., Miller, H., & Zatzepin, E. N. (1996). Structure and Mesozoic evolution of the eastern Weddell Sea, Antarctica: History of early Gondwana break-up. *Geological Society Special Publication*, *108*(1), 175–190. <https://doi.org/10.1144/GSL.SP.1996.108.01.13>
- Liu, H., Jezek, K. C., Li, B., & Zhao, Z. (2015). Radarsat antarctic mapping project digital elevation model. (NSIDC-0082, Version 2) [Dataset]. NASA National Snow and Ice Data Center Distributed Active Archive Center. <https://doi.org/10.5067/8JKNEW6BFRVD>
- Matsuoka, K., Skoglund, A., Roth, G., de Pomereu, J., Griffiths, H., Headland, R., et al. (2021). Quantarctica, an integrated mapping environment for Antarctica, the Southern Ocean, and sub-Antarctic islands. *Environmental Modelling & Software*, *140*, 105015. <https://doi.org/10.1016/j.envsoft.2021.105015958>
- Miller, H. (1990). Revised interpretation of tectonic features in the southern Weddell Sea, Antarctica, from new seismic data. *Polarforschung*, *60*, 33–38. Retrieved from <https://epic.awi.de/id/eprint/2141/>

- Müller, R. D., Gohl, K., Cande, S. C., Goncharov, A., & Golynsky, A. V. (2007). Eocene to Miocene geometry of the West Antarctic Rift System. *Australian Journal of Earth Sciences*, *54*, 1033–1045. <https://doi.org/10.1080/081200907016156911001>
- O'Brien, P. E., & Harris, P. T. (1996). Patterns of glacial erosion and deposition in Prydz Bay and the past behaviour of the Lambert Glacier. *Papers and Proceedings of the Royal Society of Tasmania*, *130*(2), 79–85. <https://doi.org/10.26749/rstpp.130.2.79>
- Rossetti, F., Storti, F., Busetti, M., Lisker, F., Vincenzo, G. D., Läufer, A. L., et al. (2006). Eocene initiation of Ross Sea dextral faulting and implications for East Antarctic neotectonics. *Journal of the Geological Society*, *163*(1), 119–126. <https://doi.org/10.1144/0016-764905-005>
- Solari, M. A., Hervé, F., Martinod, J., Roux, J. P. L., Ramírez, L. E., & Palacios, C. (2008). Geotectonic evolution of the Bransfield Basin, Antarctic Peninsula: Insights from analogue models. *Antarctic Science*, *20*(2), 185–196. <https://doi.org/10.1017/S095410200800093X>
- Uenzelmann-Neben, G., & Gohl, K. (2012). Amundsen Sea sediment drifts: Archives of modifications in oceanographic and climatic conditions. *Marine Geology*, *299–302*, 51–62. <https://doi.org/10.1016/j.margeo.2011.12.007>